



HAL
open science

Luminescent peptide/lanthanide(III) complex conjugates with push-pull antennas: application to one and two-photon microscopy imaging

Ji-Hyung Choi, Guillaume Fremy, Thibault Charnay, Nour Fayad, Jacques Pécaut, Sule Erbek, Niko Hildebrandt, Véronique Martel-Frchet, Alexei Grichine, Olivier Sénèque

► To cite this version:

Ji-Hyung Choi, Guillaume Fremy, Thibault Charnay, Nour Fayad, Jacques Pécaut, et al.. Luminescent peptide/lanthanide(III) complex conjugates with push-pull antennas: application to one and two-photon microscopy imaging. *Inorganic Chemistry*, 2022, 61 (50), pp.20674-20689. 10.1021/acs.inorgchem.2c03646 . hal-03876477

HAL Id: hal-03876477

<https://hal.science/hal-03876477>

Submitted on 8 Dec 2022

HAL is a multi-disciplinary open access archive for the deposit and dissemination of scientific research documents, whether they are published or not. The documents may come from teaching and research institutions in France or abroad, or from public or private research centers.

L'archive ouverte pluridisciplinaire **HAL**, est destinée au dépôt et à la diffusion de documents scientifiques de niveau recherche, publiés ou non, émanant des établissements d'enseignement et de recherche français ou étrangers, des laboratoires publics ou privés.



Distributed under a Creative Commons Attribution 4.0 International License

Luminescent Peptide/Lanthanide(III) Complex Conjugates with Push-Pull Antennas: Application to One and Two-Photon Microscopy Imaging

Ji-Hyung Choi,^{a‡} Guillaume Fremy,^{ab‡} Thibault Charnay,^a Nour Fayad,^c Jacques Pécaut,^d Sule Erbek,^{ef} Niko Hildebrandt,^c Véronique Martel-Frchet,^{ef} Alexei Grichine^e and Olivier Sèneque^{*a}

^a Univ. Grenoble Alpes, CNRS, CEA, IRIG, LCBM (UMR 5249), F-38000 Grenoble, France.

^b Univ. Grenoble Alpes, CNRS, DCM (UMR 5250) F-38000 Grenoble, France.

^c Laboratoire COBRA (Chimie Organique, Bioorganique, Réactivité et Analyse), UMR 6014, CNRS, Université de Rouen Normandie, INSA, Mont-Saint-Aignan cedex 76821, France.

^d Univ. Grenoble Alpes, CEA, CNRS, IRIG, SyMMES, F-38000 Grenoble, France.

^e Univ. Grenoble Alpes, INSERM U1209, CNRS UMR 5309, Institute for Advanced Biosciences, F-38000 Grenoble, France.

^f EPHE, PSL Research University, 4-14 rue Ferrus, 75014 Paris, France

Email: olivier.seneque@cea.fr

[‡] JHC and GF contributed equally to this work.



<https://creativecommons.org/licenses/by/4.0/>

This research was funded, in part, by Agence Nationale de la Recherche, Grant ANR-18-CE06-0022. A CC-BY public copyright license has been applied by the authors to the present document and will be applied to all subsequent versions up to the Author Accepted Manuscript arising from this submission, in accordance with the grant's open access conditions.

Abstract

Lanthanide(III) (Ln^{3+}) complexes feature desirable luminescence properties for cell microscopy imaging but cytosolic delivery of Ln^{3+} complexes and their use for 2P imaging of live cells are challenging. In this article, we describe the synthesis and spectroscopic characterizations a series of Ln^{3+} complexes based on two ligands, **L1** and **L2**, featuring an extended picolinate push-pull antennas for longer wavelength absorption and 2P absorption properties as well as a free carboxylate function for conjugation to peptides. Several cell penetrating peptide / Ln^{3+} complex conjugates were then prepared with the most interesting luminescence properties, Tb(**L1**) and Eu(**L2**) and with two CPPs, ZF5.3 and TP2. A spectroscopic analysis demonstrates that the luminescence properties of the complexes are not affected by conjugation to the peptide. The conjugates were evaluated for one-photon (1P) time-gated microscopy imaging, which suppresses biological background fluorescence, and 2P confocal microscopy. Whereas TP2-based conjugates were unable to enter cells, successful 1P and 2P imaging was performed with **ZF5.3[Tb(L1)]**. 2P confocal imaging suggests proper internalization and cytosolic delivery as expected for this CPP. Noteworthy, 2P confocal microscopy also allowed characterization of the luminescence properties of the complex (spectrum, lifetime) within the cell opening the way to functional luminescent probes for 2P confocal imaging of live cells.

Keywords

Peptide – Lanthanide – Conjugates – Luminescence – Microscopy

Introduction

Most lanthanide(III) cations (Ln^{3+}) present fantastic luminescence properties¹ that have pushed forward the development of luminescent lanthanide bioprobes (LLBs) during the past 30 years for applications in selective analyte detection, bioassays or cell and small animal imaging.^{2–11} The desirable properties include (i) atom-like narrow emission bands at fixed wavelengths, characteristic of each Ln^{3+} and independent of their environment, (ii) long luminescence lifetimes in the μs to ms range, which allow suppression of biological background emission by time-gated experiments for high-sensitivity detection, and (iii) low tendency to photobleaching compared to organic dyes. However, because f-f transitions are forbidden, molar absorption coefficients of Ln^{3+} are very weak ($< 3 \text{ M}^{-1} \text{ cm}^{-1}$) precluding their efficient direct excitation. Nevertheless, efficient excitation of Ln^{3+} can be achieved using a proximal light-harvesting chromophore able to transfer, after excitation, electronic energy to the Ln^{3+} in order to populate its emissive excited states. This phenomenon is referred to as the “antenna effect” and often results in a large difference between excitation and emission wavelengths, which avoids self-absorption problems. The antenna depends on the Ln^{3+} : its excited donor state must be energetically close enough to the Ln^{3+} excited state for efficient electronic energy transfer, but not too close to avoid thermally-activated back energy transfer from the Ln^{3+} to the antenna. As a rule of thumb, the antenna donor excited state must stand *ca.* 2000–5000 cm^{-1} above the Ln^{3+} excited emissive state. Besides Ln^{3+} and its sensitizing antenna, the third component of LLBs is a chelating ligand. In order to reduce non-radiative de-excitation arising from water molecules coordinated to the Ln^{3+} , this ligand must saturate as much as possible the coordination sites around Ln^{3+} . For biological applications, these complexes must be thermodynamically stable and kinetically inert.

Combining luminescence properties of lanthanide complexes and selective recognition or targeting properties of peptides or proteins is an interesting design option for responsive probes,^{12–25} bioassays^{26,27,7,28} or cellular imaging.^{29–33} During the past 15 years, a large effort has been devoted to the development of LLBs suitable for cell microscopy imaging. The groups of Parker^{32–44} and Maury^{45–54} have been particularly active in this field, describing neutral or positively charged macrocyclic Ln complexes with sensitizing antennas that could stain fixed or live cells. Complexes enter live cells by active uptake mechanisms and most often end up in lysosomes or stick to mitochondria membranes. Topological elements of the ligand, such as antenna chromophore nature, point of attachment and linker length to coordinating groups, and the number of pendant arms, play a major role in determining the complex localization. However, controlled delivery within the cytosol or within a specific and chosen organelle is hardly achieved.^{33,37,43} During the past years, several peptides have been reported to efficiently deliver their conjugated cargo (a fluorophore, a drug, an active protein) to the cytoplasm of live cells.^{55–60} Therefore, conjugating lanthanide complexes to such peptides is an interesting approach in order to better control cell internalization and localization of the LLB.

Two strategies are possible to prepare peptide/lanthanide complex conjugates. The first one relies on chemoselective reaction between a water-soluble peptide and a lanthanide complex using click chemistry reactions (post resin-cleavage conjugation).^{33,61–63} It consists in the following sequence: (i) synthesis of the peptide by solid phase peptide synthesis (SPPS); (ii) cleavage of the peptide from the resin and removal of side chain protecting groups; (iii) conjugation in water using suitable reactive groups on peptide and lanthanide complex. The synthesis is straightforward but the main disadvantages are (i) the requirement of water-soluble Ln^{3+} complexes and (i) high concentrations of peptide and/or Ln^{3+} complex may be needed for efficient conjugation. The alternative strategy involves grafting of the chelate onto the peptide on resin (pre-resin cleavage conjugation) as follows: (i) synthesis of the peptide by SPPS, inserting in the sequence an amino acid (lysine, glutamate) in the sequence with an orthogonally protected side chain; (ii) selective removal of this protecting group; (iii) on-resin coupling of a

protected chelate; (iv) cleavage of the peptide from the resin as well as removal of side-chain and chelate protecting groups, and (v) metalation of the peptide-bound chelate by Ln^{3+} .^{15,21,22,64} The advantage of this strategy is that all the synthesis is performed on resin with a single purification step at the end. However, it requires a chelate with some coordinating moieties protected to leave a single reactive function for coupling to lysine or glutamate. Common partly protected chelates for this pre-resin cleavage conjugation are DOTA-*tris*(*t*Bu)ester,⁶⁵ DOTAGA-*tetra*(*t*Bu)ester,⁶⁶ or DTPA-*tetra*(*t*Bu)ester.⁶⁷ These protected chelates generally lack an antenna moiety, which requires introduction of a remote antenna somewhere else on the peptide to create luminescent probes. Recently, we have described the DO3Apic-*tris*(*t*Bu)ester and DO3Apic-*tris*(allyl)ester protected chelates suitable for the preparation of peptide/ Ln^{3+} complex conjugates with a picolinate Ln^{3+} -coordinating moiety able to act as an antenna to sensitize Ln^{3+} luminescence.⁶⁸ However, absorption of the picolinate moiety is far in the UV with a maximum at 280 nm, which is not suitable for most biological applications, especially cellular imaging.

In this article, we describe the synthesis and spectroscopic characterization of a family of $[\text{Ln}(\text{DO3Apic})]$ complexes with extended picolinate antenna for longer wavelength excitation and with an appended carboxylate function for conjugation to a lysine side chain *via* the pre-resin cleavage conjugation strategy. Inspired by the group of Maury, we developed ligands **L1** and **L2** and their protected derivatives **L1(Me)₄** and **L2(Me)₄** for on-resin peptide conjugation (Figure 1). **L1** features an aryl-picolinate twisted push-pull antenna with an O-donor that has been shown to sensitize Tb^{3+} or Dy^{3+} luminescence efficiently with a charge transfer (CT) absorption band at 305 nm (λ_{max}) and extending up to 350 nm.^{53,54} **L2** features an aryl-alkyne-picolinate push-pull antenna with an O-donor. Such an antenna is suitable for Eu^{3+} and Sm^{3+} sensitization with a CT band around 330 nm extending up to 380 nm.^{54,69} These push-pull antennas present two-photon (2P) absorption properties that allowed 2P microscopy imaging of fixed cells by the Maury group. We prepared several conjugates of cell penetrating peptides and **L1** and **L2** and assessed their potential for live cell microscopy imaging.

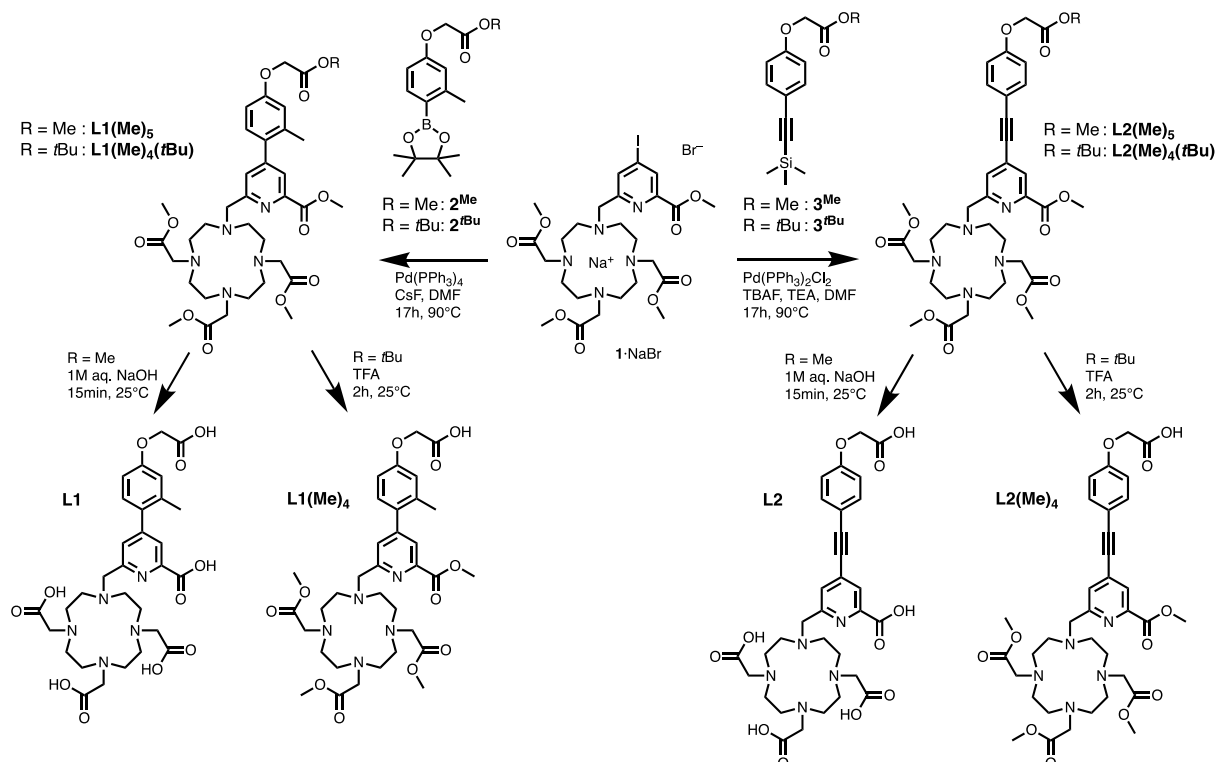


Figure 1. Synthetic pathways for ligand **L1** and **L2** and partially protected building blocks for conjugation **L1(Me)₄** and **L2(Me)₄**.

Results and discussion

Synthesis and photophysical properties of [Ln(DO3Apic)]⁻ complexes with extended picolinate antenna. First, Ln³⁺ complexes of **L1** and **L2** were synthesized and their spectroscopic properties were evaluated. A common precursor of **L1** and **L2** is iodinated compound **1**·NaBr (Figure 1), which was prepared on a large scale by reaction of [1,4,7-*tris*(methoxycarbonylmethyl)]-1,4,7,10-tetraazacyclododecane hydrobromide⁷⁰ with methyl 4-iodo-6-(((methylsulfonyl)oxy)methyl)picolinate (see details in SI).⁴⁸ Crystals of **1**·NaBr suitable for X-ray diffraction were obtained by slow evaporation of a methanol solution of the compound. The X-ray structure shows a Na⁺ ion bound to the four nitrogen atoms of the cyclen macrocycle, the nitrogen atom of the picolinate unit, and three oxygen atoms from two methyl-acetate arms and the picolinate methyl ester (Figure 2A). This leaves one methyl-acetate arm unbound. Then, **1**·NaBr was converted into **L1(Me)₅** or **L2(Me)₅** by Suzuki-Miyaura coupling with **2^{Me}** or Sonogashira coupling with **3^{Me}**, respectively (Figure 1). The Suzuki-Miyaura coupling is performed in the presence of CsF to generate *in situ* the more reactive trifluoroborate intermediate. The Sonogashira coupling is performed under modified conditions: (i) in the absence of Cu(I) to avoid formation of macrocycle-copper complex that cannot be purified and (ii) with *in situ* deprotection of the alkyne-TMS reagent by tetrabutylammonium fluoride (TBAF). Subsequent hydrolysis of the five methyl esters by NaOH gave **L1** and **L2** in 60% and 47% yield, respectively, over the two steps. Reaction of **L1** or **L2** with LnCl₃ (Ln = Tb, Eu and Dy for **L1**; Ln = Eu and Sm for **L2**) in water in the presence of triethylamine yielded >98% pure [Ln(L)](Et₃NH) (**L** = **L1** or **L2**) after precipitation in acetone as shown by HPLC analysis (Figure S2 and S3 of ESI). In all cases, high resolution mass spectrometry confirmed the formation of anionic [Ln(L)]⁻ compounds. Single crystals suitable for X-ray crystallography were obtained by slow evaporation of a methanol solution of [Tb(**L1**)]⁻. The crystal structure (Figure 2B,C) shows two [Tb(**L1**)]⁻ units bridged by two tris-hydrated Na⁺ cations coordinated by the carboxylate of the picolinate moiety. The Tb³⁺ ion is nona-coordinated by the five nitrogen atoms from the cyclen and the pyridine ring as well as four oxygen atoms from the three acetate arms and from the picolinate moiety. A 40.4 (3) degrees twist angle is observed between the pyridine and the aryl rings of the antenna moiety. The carboxylic acid on the O-donor group of the antenna is in its protonated form.

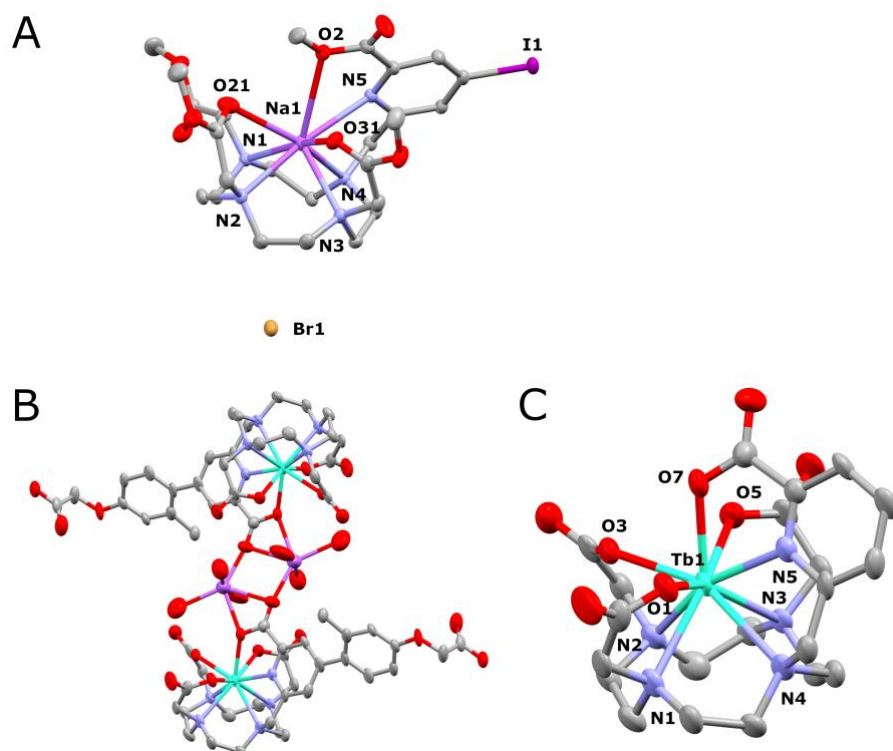


Figure 2. (A) X-ray structure of **1**·NaBr with C in grey, N in blue, O in red, Na in pink, and I in purple. Selected distances (Å): Na1···N1 2.630 (2), Na1···N2 2.532 (2), Na1···N3 2.573 (2), Na1···N4 2.610 (2), Na1···N5 2.612 (2), Na1···O2 2.962 (2), Na1···O21 2.730 (2), Na1···O31 2.585 (2). (B) X-ray structure of ([Tb(**L1**)]Na(H₂O)₃)₂ with C in grey, N in blue, O in red, Na in pink and Tb in cyan. (C) Enlarged view of the Tb(DO3Apic) moiety. Selected distances (Å): Tb1···N1 2.617 (6), Tb1···N2 2.653 (7), Tb1···N3 2.689 (6), Tb1···N4 2.723 (6), Tb1···N5 2.504 (6), Tb1···O1 2.348 (5), Tb1···O3 2.340 (5), Tb1···O5 2.361 (5), Tb1···O7 2.397 (5). Hydrogens are omitted for clarity. Ellipsoids are shown at the 50% probability level.

The spectroscopic properties of the Ln³⁺ complexes were studied in HEPES buffer (10 mM, pH 7.5). Absorption, excitation and emission spectra are displayed in Figure 3 and spectroscopic data are summarized in Table 1. The absorption spectrum of [Tb(**L1**)]⁻ shows two maxima at 290 and 305 nm assigned to transitions to a locally excited state (LE) and an intra-ligand charge transfer excited state (ILCT), respectively.⁵³ Excitation at 305 nm results in characteristic Tb³⁺ emission with intense ⁵D₄ → ⁷F_J (*J* = 6, 5, 4, 3) at 490, 545, 585, and 620 nm, respectively, and weaker ⁵D₄ → ⁷F_J (*J* = 2, 1, 0) at 650, 665, and 680 nm, respectively. The excitation spectrum is similar to the absorption spectrum, indicating that Tb³⁺ luminescence sensitization arises from excitation of both the π-π* and the ILCT transitions. The Tb³⁺ luminescence lifetime, τ_{Tb}, is long (2.35 ms, mono-exponential decay) and the quantum yield of sensitized Tb³⁺ emission, Φ_{Tb}, is 0.62, which is high and comparable to those reported for related Tb³⁺ complexes with the same antenna but based on tacn (1,4,7-triazacyclononane, Φ_{Tb} = 0.74) or pyclen (1,4,7,10-tetraaza-2,6-pyridinophane, Φ_{Tb} = 0.72) macrocycles. The hydration number *q* was determined to be zero from the Tb³⁺ lifetime differences in H₂O and D₂O.^{71,72} In agreement with the crystal structure, no Tb³⁺-bound water molecule is found. Furthermore, **L1** is also able to sensitize the emission of Eu³⁺, with characteristic ⁵D₀ → ⁷F_J (*J* = 0, 1, 2, 3, 4) transitions at 580, 590, 615, 650, and 700 nm, and Dy³⁺, with characteristic ⁴F_{9/2} → ⁶H_J (*J* = 15/2, 13/2, 11/2) transitions at 475, 575, and 660 nm as expected for this aryl-picolinate antenna with O-alkyl substituent.⁵²⁻⁵⁴ However, the quantum yields of [Eu(**L1**)]⁻ and [Dy(**L1**)]⁻ are 0.064 and 0.012, respectively, which is significantly weaker than for their Tb³⁺ analogue. A *q* = 0 value was confirmed for [Eu(**L1**)]⁻ as well from measurements in H₂O and D₂O.^{72,73}

[Eu(L2)]⁻ displays an absorption band at 335 nm attributed to an ILCT transition.^{54,74} Excitation into this band induces Eu³⁺ emission. The Eu³⁺ emission lifetime is long (1.09 ms, mono-exponential decay) and complementary measurements in D₂O confirm that no water molecule is bound to the Eu³⁺ ion. The quantum yield of sensitized Eu³⁺ emission, Φ_{Eu} , is 0.17. Both lifetime and quantum yield of [Eu(L2)]⁻ are comparable with those of related compounds with a pyridinephosphinate arm instead of a pyridinecarboxylate arm.⁷⁵ As already shown, aryl-alkynyl-picolinate antennas with O-alkyl donor can sensitize Sm³⁺ emission.⁴⁹ Upon excitation at 335 nm, [Sm(L2)]⁻ displays characteristic Sm³⁺ emission with ⁴G_{5/2} → ⁵H_{*J*} (*J* = 5/2, 7/2, 9/2, 11/2) transitions at 565, 600, 645, and 700 nm as well as a broad residual ligand-centered emission at λ_{max} = 457 nm. The lifetime of Sm³⁺ emission is short (\approx 0.02 μ s) and the quantum yield is low (Φ_{Sm} = 0.004).

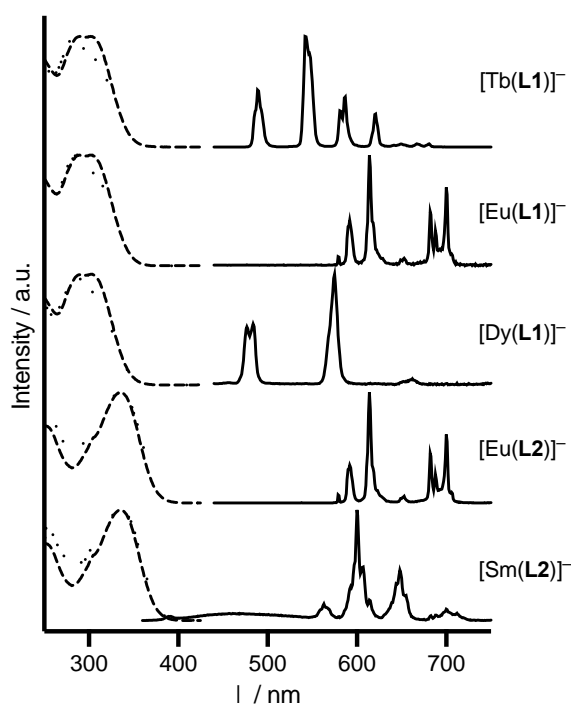


Figure 3. Normalized absorption (dashed line), excitation (dotted line), and emission (solid line) spectra of complexes [Tb(L1)]⁻, [Eu(L1)]⁻, [Dy(L1)]⁻, [Eu(L2)]⁻, [Sm(L2)]⁻ in HEPES buffer (10 mM, pH 7.5). Emission spectra were recorded with excitation at 303 and 335 nm for [Ln(L1)]⁻ and [Ln(L2)]⁻ complexes, respectively. Excitation spectra were recorded with emission at 545, 615, 570 and 600 nm for Tb³⁺, Eu³⁺, Dy³⁺, and Sm³⁺, respectively.

Table 1. Spectroscopic data for [Ln(L1)]⁻ and [Ln(L2)]⁻ complexes and conjugates.^a

	$\lambda_{\text{abs}} / \text{nm}$	$\epsilon / \text{M}^{-1} \text{cm}^{-1}{}^b$	$\tau_{\text{Ln}} (\text{H}_2\text{O}) / \text{ms}^c$	$\tau_{\text{Ln}} (\text{D}_2\text{O}) / \text{ms}$	q^d	Φ_{Ln}^e
[Tb(L1)] ⁻	303	12 000	2.35	2.47	0.1 / -0.2	0.62
[Eu(L1)] ⁻	303	12 000	1.10	1.66	0.0 / 0.1	0.064
[Dy(L1)] ⁻	303	12 000	0.10	n.d. ^f	n.d.	0.012
[Eu(L2)] ⁻	335	28 200	1.09	1.61	0.0 / 0.1	0.17
[Sm(L2)] ⁻	335	28 200	\approx 0.02	n.d.	n.d.	0.004
TP2[Tb(L1)]	303	12 000	2.41	2.52	0.1 / -0.2	0.61
TP2[Eu(L2)]	335	28 200	1.07	1.60	0.0 / 0.1	0.15
ZF5.3[Tb(L1)]	303	12 000	2.32	n.d.	n.d.	0.61

^a Measurements were performed in HEPES buffer (10 mM, pH 7.5) except lifetimes in D₂O that were measured in unbuffered deuterated water. ^b Uncertainty on ϵ values is estimated $\pm 500 \text{ M}^{-1} \text{ cm}^{-1}$. Values of ϵ for conjugates are assumed identical to those of [Ln(L1)]⁻ or [Ln(L2)]⁻ complexes as the peptide scaffold has no absorption above 300 nm. ^c Error on lifetime decay values is $\pm 0.03 \text{ ms}$. ^d q values were determined using Horrocks' equations^{71,73} (left-hand side values), $q^{\text{Tb}} = 4.2 \times (1/\tau(\text{H}_2\text{O}) - 1/\tau(\text{D}_2\text{O}))$ and $q^{\text{Eu}} = 1.11 \times (1/\tau(\text{H}_2\text{O}) - 1/\tau(\text{D}_2\text{O}) - 0.31)$ for Tb³⁺ and Eu³⁺, respectively, and using Parker's equations⁷² (right-hand side value), $q^{\text{Tb}} = 5.0 \times (1/\tau(\text{H}_2\text{O}) - 1/\tau(\text{D}_2\text{O}) - 0.06)$ and $q^{\text{Eu}} = 1.2 \times (1/\tau(\text{H}_2\text{O}) - 1/\tau(\text{D}_2\text{O}) - 0.25)$ for Tb³⁺ and Eu³⁺, respectively, with τ in ms. Uncertainty on q values from these empirical equations is estimated ± 0.3 . ^e Estimated error on Φ_{Ln} values is $\pm 10\%$. ^f Not determined.

Synthesis and photophysical properties of peptide/lanthanide complex conjugates. Since L1 and L2 provide luminescent Ln³⁺ complexes with interesting properties, especially with Tb³⁺ and Eu³⁺, Tb(L1) and Eu(L2) complexes were conjugated to cell penetrating peptides (CPP) and evaluated for live cell imaging. As CPPs, we selected two peptides reported to reach the cytosol of live cells: TP2, a spontaneous membrane translocating peptide,⁶⁰ and ZF5.3, a zinc finger peptide featuring a peculiar penta-arginine motif, referred to as 5.3, that promotes early-endosome escape.^{59,76} Compared to the ZF5.3 sequence described by Schepartz et al.,^{59,76} the N-terminal WY motif was changed for an AF motif because the former two amino acids have an absorption band around 280 nm (extending up to 300 nm and 310 nm for Y and W, respectively) that overlaps the absorption of L1. In the case of TP2, the Y residue was conserved as it is presumably essential for penetration properties.⁶⁰ The peptide sequences used in this study are given in Figure 4A. First, we prepared analogues of L1 and L2 with the four Ln³⁺-binding carboxylates protected as methyl esters, namely L1(Me)₄ and L2(Me)₄ (Figure 1), that could be used for conjugation to a peptide through the carboxylic acid of the antenna O-donor group. In this respect, 2^{tBu} and 3^{tBu} were reacted with 1·NaBr by Suzuki-Miyaura and Sonogashira coupling (same conditions as mentioned above), respectively, to give L1(Me)₄(tBu) and L2(Me)₄(tBu). Acidolysis of the tBu ester in TFA yielded L1(Me)₄ and L2(Me)₄. The pathway for the preparation of conjugate TP2[Tb(L1)] is displayed in Figure 4B. Peptide TP2 was synthesized on Rink Amide resin by SPPS using Fmoc/tBu chemistry. A lysine protected with an Alloc group, orthogonal to other protecting groups, was used as the C-terminal amino acid. The N-terminus was protected by a Boc group. Selective Alloc removal was performed on resin using a Pd⁰ catalyst. L1(Me)₄ was then coupled to the free C-terminal lysine side chain using PyBOP/DIEA activation. Treatment of the resin with a mixture of TFA and scavengers (H₂O, triisopropylsilane and thioanisole) yielded TP2[L1(Me)₄] featuring the chelate with methyl ester arms. Hydrolysis of the methyl esters was performed using 0.1 M NaOH for 2 h to give TP2[L1]. Subsequent metalation with TbCl₃ in water at pH 7.5 yielded TP2[Tb(L1)]. TP2[Eu(L2)] and ZF5.3[Tb(L1)] were obtained in a similar way. Note that Ln³⁺ remains bound to the chelate in the acidic conditions used for HPLC purifications (eluent contained 0.1% TFA, pH \approx 2): the conjugates are stable in these conditions. Details concerning the synthesis of the three conjugates, including final HPLC chromatogram and ESI-MS analysis are given in the ESI.

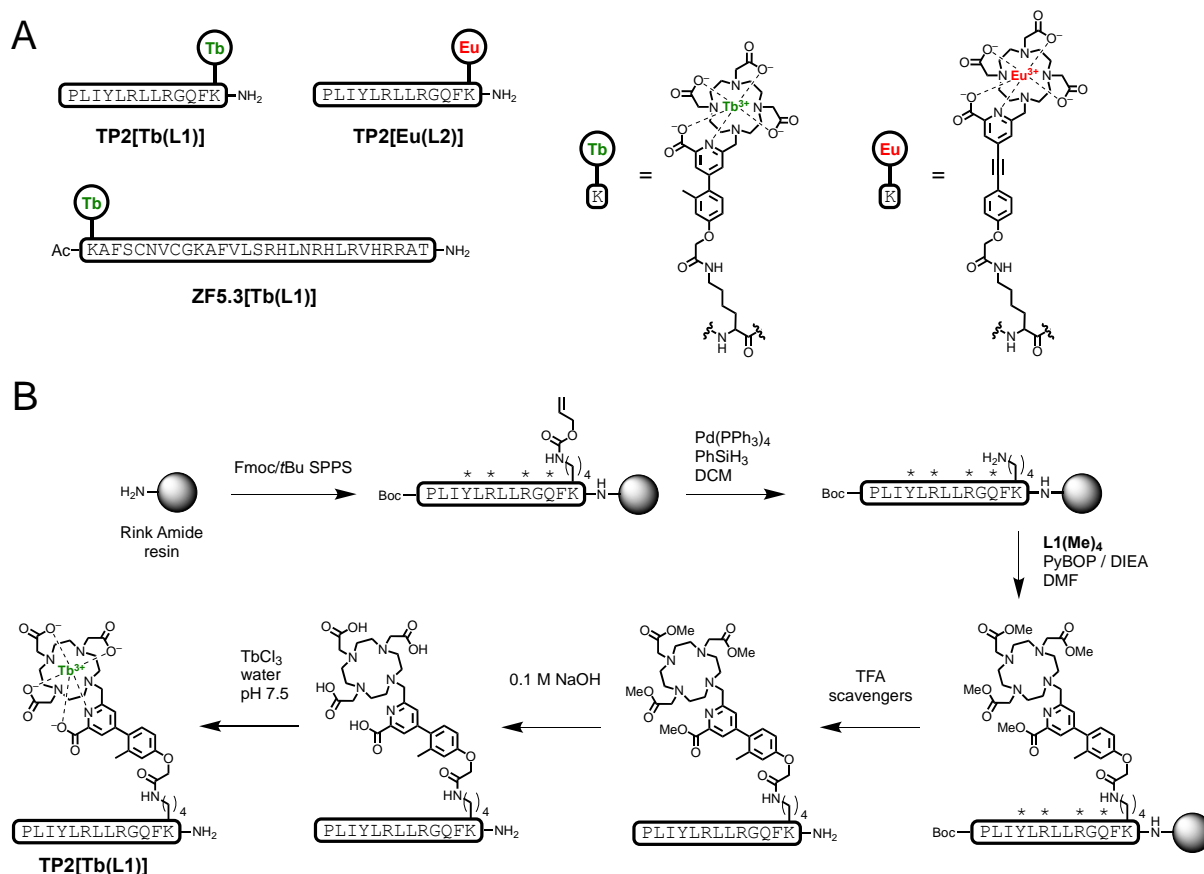


Figure 4. (A) Amino acid sequence of conjugates **TP2[Tb(L1)]**, **TP2[Eu(L2)]**, and **ZF5.3[Tb(L1)]**. (B) Synthetic pathway for **TP2[Tb(L1)]**. * denotes standard side chain protecting group (*t*Bu for Tyr; Pbf for Arg; Trt for Gln).

The photophysical properties of the three conjugates were investigated in HEPES buffer (10 mM, pH 7.5). For **ZF5.3[Tb(L1)]**, TCEP (*tris*(carboxyethyl)phosphine, 250 μ M) and Zn^{2+} (2 eq. vs peptide) were added in the buffer to ensure reduction of the cysteine and folding of the zinc finger peptide through Zn binding, respectively. All of them display characteristic Tb^{3+} or Eu^{3+} emission and their emission and excitation spectra are identical to those of the parent $[Tb(L1)]^-$ or $[Eu(L2)]^-$ complexes (Figure 5). The Tb^{3+} luminescence lifetimes of **TP2[Tb(L1)]** and **ZF5.3[Tb(L1)]** are 2.41 (3) and 2.32 (3) ms (Table 1), respectively, which is very similar to the lifetime of $[Tb(L1)]^-$ (2.35 (3) ms). In agreement, quantum yields of **TP2[Tb(L1)]** and **ZF5.3[Tb(L1)]** ($\Phi_{Tb} = 0.61$ for both conjugates) are almost identical to the one of $[Tb(L1)]^-$ ($\Phi_{Ln} = 0.62$). The Eu^{3+} luminescence lifetime and quantum yield of **TP2[Eu(L2)]** are also the same as those of $[Eu(L2)]^-$ within margin error. For the three conjugates there is no water molecule in the Ln^{3+} coordination sphere as shown by the q values (Table 1). All these results indicate that conjugation to the peptide has no influence on the luminescence properties of the Ln^{3+} complex.

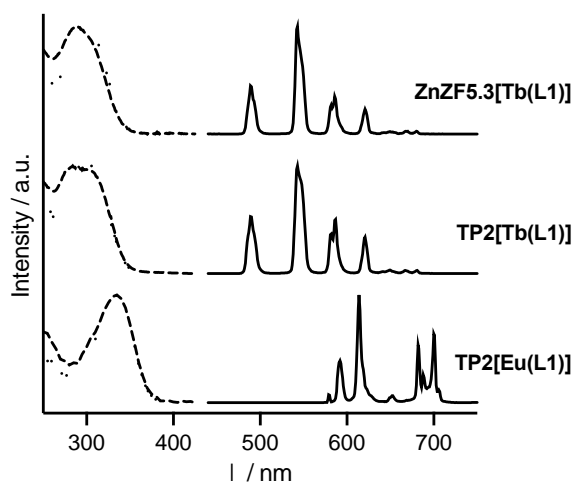


Figure 5. Normalized absorption (dashed line), excitation (dotted line) and emission (solid line) spectra of **TP2[Tb(L1)]**, **TP2[Eu(L2)]**, and **ZF5.3[Tb(L1)]** in HEPES buffer (10 mM, pH 7.5). Emission spectra were recorded with excitation at 303 and 335 nm for Tb^{3+} and Eu^{3+} compounds, respectively. Excitation spectra were recorded with emission at 545 and 615 nm for Tb^{3+} and Eu^{3+} , respectively.

It should be noted that we also tried to synthesize **ZF5.3[Eu(L2)]** but we encountered several problems. First, we noticed addition of thioanisole onto the peptide (mass increase of 124) during resin cleavage with a TFA / H_2O / triisopropylsilane / thioanisole mixture. This was not observed for **ZF5.3[Tb(L1)]**, suggesting addition of thioanisole on the alkyne function of the antenna during TFA/scavenger treatment. Removing thioanisole from the cleavage cocktail yielded a peptide with the expected mass for **ZF5.3[L2(Me)₄]**. However, the Eu^{3+} conjugate obtained at the end of the synthesis was unable to bind Zn^{2+} and displayed red-shifted absorption (*ca.* 20 nm) of the antenna compared to $[\text{Eu}(\text{L2})]^-$ or **TP2[Eu(L2)]**. In the meantime, we attempted the synthesis of a related conjugate with **Eu(L2)** as a Ln complex. This peptide contained a single cysteine. Again, the antenna absorption was red-shifted. We performed a DTNB assay on this peptide to measure free thiol content and found no free thiol despite the correct mass. This is consistent with thiol addition onto the triple bond of the antenna (thiol-yne reaction). Therefore, it seems that alkyne-containing antennas are prone to reaction with sulphur compounds (sulphides or thiols), which prevents their use with peptides comprising cysteine or methionine.

Cellular imaging. Time-gated microscopy is a convenient technique for cellular imaging of cells with Ln probes because it suppresses biological background fluorescence.²⁹ Monophotonic (1P) time-gated photoluminescence microscopy was attempted with conjugates **TP2[Tb(L1)]**, **TP2[Eu(L2)]**, and **ZF5.3[Tb(L1)]** in order to benefit from the long luminescence lifetime of Ln^{3+} ions to suppress biological background fluorescence. Mouse NIH3T3 cells were incubated 4 h with each of the conjugates (10 μM) then rinsed and studied under the microscope with 1P pulsed excitation at 337 nm and a 100 μs delay (after the excitation pulse) and 3 ms gate-width time. In the case of the TP2 conjugates, PBS incubation buffer contained 1% DMSO as described in the literature.^{60,77} Diffuse luminescence emission was observed from NIH3T3 cells incubated with **ZF5.3[Tb(L1)]** as shown in Figure 6A. The 100 μs delay time and the 543 nm band-pass filter used ensures that emission originates from Tb^{3+} . Owing to the reported internalization properties of **ZF5.3**,^{59,76} this suggests proper internalization of **ZF5.3[Tb(L1)]** in NIH3T3 cells. However, some of the cells do not display Tb^{3+} emission and for those with Tb^{3+} emission, the emitted intensity seems to vary depending on cell, indicating non-uniform internalization. On the contrary to **ZF5.3[Tb(L1)]**, no luminescence could be detected with **TP2[Tb(L1)]** and

TP2[Eu(L2)] conjugates. It was reported that the polarity of the fluorescent cargo attached to the TP2 peptide has strong impact on membrane translocation efficiency.⁷⁷ The negatively charged Ln(DO3Apic) complex is probably too polar and precludes membrane translocation in the case of TP2. On the contrary, ZF5.3 was reported to internalize cargoes of various size, from small fluorophore to large proteins.^{59,76,78} Its delivery properties seems to be less influenced by the nature of its cargo and the negatively charged Ln(DO3Apic) complex does not impair its function. In the case of TP2, the luminophore is very close to the peptide motif that promotes cell penetration while in ZF5.3, it is farther. This might explain the lower influence of the cargo for the latter.

Despite the low repetition rates and very short excitation pulses, UV excitation used for 1P microscopy is potentially phototoxic. Tb³⁺ complexes with the same antenna as [Tb(L1)]⁻ have been successfully used by the group of Maury for biphotonic (2P) confocal microscopy imaging of cells.^{53,54} Therefore, 2P imaging was attempted with **ZF5.3[Tb(L1)]**, but using a different cell strain. HeLa cells were incubated 3 h with the conjugate (10 μM) in PBS buffer, rinsed, and imaged under 2P excitation at 700 nm. As seen in Figure 6B, a diffuse luminescence emission was detected in cells together with more intense emission spots, appearing as light streaks in the image (*vide infra*). This emission could be unambiguously attributed to Tb³⁺ emission based on spectral analysis. Figure 6C shows emission spectra recorded in different areas: whole cell, intense spots and diffuse signal. All three are characteristic of Tb³⁺ emission with minor autofluorescence emission (broad emission with maximum around 450 nm). Lifetime measurement were also performed in areas corresponding to diffuse signal and intense spots using the TSLIM method.⁴⁷ Lifetimes, determined by fitting the luminescence decay with a mono-exponential, were 0.99 ms and 0.78 ms for intense spots and diffuse signal, respectively. Although lower than the one measured in solution with a photoluminescence spectrometer, this long lifetime in the millisecond range confirms Tb³⁺ emission. Horizontal light streaks that are observed to the right of intense spots are due to the fact that the luminescent lifetime of the Tb³⁺ complex is much longer than the longest pixel dwell time available in raster scanning mode.⁴⁷ ZF5.3 was reported to enter cells by the endosomal pathway and to escape endosomes.^{59,76} The presence of a diffuse Tb³⁺ emission within the whole cell, attests to the successful cytosolic delivery of **ZF5.3[Tb(L1)]**. Intense spots may correspond to endosomal vesicles still containing **ZF5.3[Tb(L1)]**. As endosomal escape is a time dependent process, it remains to investigate whether complete endosomal release could be achieved with longer incubation or resting time before microscopy. Nevertheless, these results show that conjugation of luminescent Ln³⁺ complex to CPP is interesting to control their delivery into the cytosol of live cells. This behavior stands in contrast with bare Ln³⁺ complexes, i.e. devoid of CPP, that often end-up in lysosomes. However, despite Tb³⁺ emission under 2P excitation with **ZF5.3[Tb(L1)]** is detectable, it is rather weak. This may be due to the fact that we were exciting the sample at 700 nm, corresponding to the lower edge of excitation window with the Ti:Sapphire laser used. Therefore, excitation is performed in the tail of the complex 2P absorption band, and is probably very weak. Therefore, the system needs to be improved. Work is in progress to optimize the optical properties, especially by a red-shifting the excitation wavelength using antennas with more extended π systems and by enhancing the 2P absorption properties. Other cell penetrating sequences allowing cytosolic delivery will be tested and target and label specifically an organelle using signal peptide sequences would constitute an interesting extension to this approach. Nevertheless, this work constitutes a proof-of-concept of internalization of Ln³⁺ complexes with 2P absorption properties using a CPP. Work is in progress to increase 2P absorption properties of conjugated Ln³⁺ complexes, especially by red-shifting their absorption band.

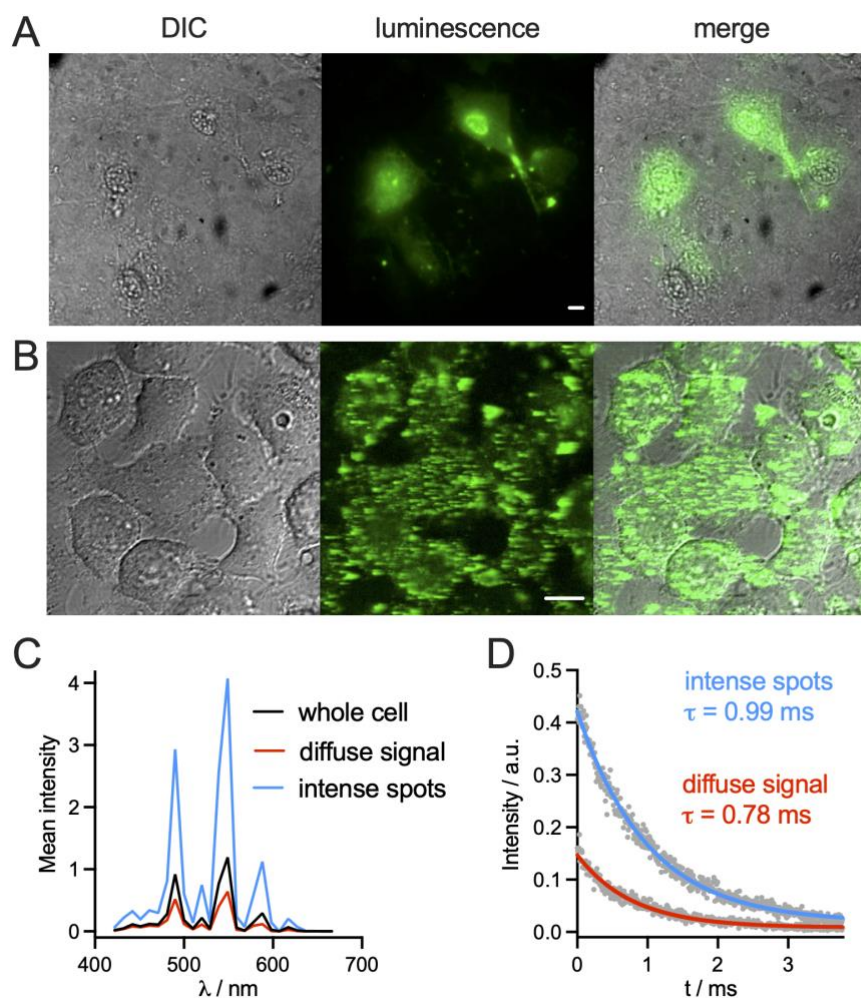


Figure 6. Cellular imaging. (A) 1P time-gated (100 μ s delay, 3 ms gate, $\lambda_{\text{ex}} = 337$ nm) photoluminescence imaging of NIH3T3 cells incubated 4 h with **ZF5.3[Tb(L1)]** (10 μ M). (B) 2P confocal imaging ($\lambda_{\text{ex}} = 700$ nm) of living HeLa cells incubated 3 h with **ZF5.3[Tb(L1)]** (10 μ M). (C) 2P-excited emission spectrum recorded in areas corresponding to whole cell, diffuse signal, and intense spots and (D) emission decay (grey) with mono-exponential fits (red for diffuse signal and blue for intense spots). For (A) and (B), Left panel shows the differential interference contrast (DIC) image, middle panel shows the luminescence image, and right panel shows the merge. Scale bar in middle panel correspond to 10 μ m.

Conclusion

To conclude, we have described a family of Ln^{3+} complexes comprising a DO3Apic ligand with extended antenna that confer long-wavelength excitation. The antenna is equipped with a carboxylate group for conjugation to peptide. Among them $[\text{Tb}(\mathbf{L1})]^-$ and $[\text{Eu}(\mathbf{L2})]^-$ display high quantum yields (0.62 and 0.17, respectively) and long luminescence lifetimes (2.35 and 1.09 ms, respectively). Peptide-Ln complex conjugates have been successfully prepared using partially protected macrocyclic ligands **L1(Me)₄** and **L2(Me)₄** and cell penetrating peptides. Tb^{3+} and Eu^{3+} conjugates display the same photophysical properties as the parent $[\text{Tb}(\mathbf{L1})]^-$ and $[\text{Eu}(\mathbf{L2})]^-$ complexes, indicating that conjugation to the peptide does not alter the luminescence properties. Nevertheless, preparation of conjugates with the alkyne-comprising ligand **L2** is not possible with peptides including cysteines due to thiol-yne reaction, which changes the antenna photophysical properties and makes it unable to sensitize Eu^{3+} luminescence (besides making cysteines no more available). To demonstrate the

applicability of the peptide-Ln complex conjugates, 1P time-gated imaging and 2P confocal live-cell imaging proof-of-concept experiments were performed with one of these conjugates, **ZF5.3[Tb(L1)]**. Successful targeting of the conjugate in the cytosol was observed and 2P imaging allowed the determination of the intracellular photophysical properties (spectra, lifetimes) of this conjugate in live cells. Additionally, our results open the way for the design of functional LLBs (e.g., responsive probes whose luminescence would be triggered by binding to an analyte) on the basis peptide/lanthanide complex conjugates with autofluorescence background suppression (time-gated imaging) and two-photon absorption properties and their use in live cells.

Experimental section

Materials and methods. *N*- α -Fmoc-protected amino acids for peptide synthesis, HCTU coupling reagent and NovaPEG Rink Amide resin were purchased from Novabiochem or Iris Biotech. Other reagents for peptide synthesis, solvents, buffers and metal salts were purchased from Sigma-Aldrich. All buffer or metal solutions for spectroscopic measurements were prepared with ultrapure water produced by a Millipore Milli-Q purification system (purified to 18.2 M Ω .cm). The concentration of the Zn²⁺ solution was determined by colorimetric EDTA titrations.⁷⁹ Buffer solutions were treated with Chelex 100 resin (Bio-Rad) to remove trace metal ions. Analytical HPLC/LRMS analyses were performed on an Agilent Infinity 1260 II system equipped with a 6125 MS (ESI) detector using a Waters XBridge BEH130 C18 (2.5 μ m, 75 mm \times 4.6 mm). Preparative HPLC separations were performed on a VWR LaPrep Σ system using Waters XBridge Peptide BEH130 C18 (5 μ m, 150 mm \times 19 mm) or Waters XBridge Peptide BEH130 C18 (5 μ m, 150 mm \times 10 mm) columns at flow rates of 14 or 6 mL/min, respectively. Mobile phase consisted in a gradient of solvent A (0.1 % trifluoroacetic acid (TFA) in H₂O) and B (0.1 % TFA in CH₃CN/H₂O 9:1). For analytical separations, Method A consisted in 5 % B during 1 min followed by a 5 to 50 % B linear gradient in 13 min at 1 mL/min and Method B consisted in 5% B during 1 min followed by a 5 to 100 % B gradient in 13 min at 1 mL/min. Eluate was monitored by electronic absorption at 214, 280 and 331 nm as well as by LRMS(ESI+) detection. ¹H, ¹³C and DEPT NMR spectra were recorded at 400 MHz on a Varian Avance III 400 spectrometer at 298 K unless specified. Coupling constants (*J*) are measured in hertz and are given with 0.5 Hz accuracy and the chemical shift (δ) are measured in ppm. All chemical shifts for ¹H and ¹³C spectra were referenced to the residual solvent peak (CDCl₃ δ _H = 7.26 ppm and δ _C = 77.2 ppm; D₂O δ _H = 4.79 ppm at 298 K and 4.20 ppm at 353 K) or external reference (sodium trimethylsilylpropanesulfonate for ¹³C spectra in D₂O). The following abbreviations were for peak multiplicities: s (singlet), d (doublet), t (triplet), q (quartet), dd (doublet of doublet), m (multiplet). LRMS(ESI) analyses were performed on a Thermo Scientific LXQ spectrometer. HRMS(ESI) were performed on a Thermo Scientific LTQ Orbitrap XL spectrometer or on a Waters Xevo G2-S QToF spectrometer with electrospray ionization. UV-Vis absorption spectra were recorded on a Perkin-Elmer Lambda 35 spectrophotometer or on a Varian Cary 50 spectrometer, both equipped with a thermo-regulated cell holder.

Luminescence. Luminescence spectra were measured on a Varian Cary Eclipse spectrometer equipped with a thermo-regulated cell holder or on a modular Fluorolog FL3-22 spectrometer from Horiba-Jobin Yvon-Spex equipped with a double-grating excitation monochromator and an iHR320 imaging spectrometer coupled to Hamamatsu R928P and Hamamatsu R5509 photomultipliers for visible and NIR detection, respectively. Emission spectra were corrected for wavelength-dependent detector response. Time-gated Ln³⁺ luminescence spectra were acquired with 100 μ s time delay and 2 ms gate time on the Varian Cary Eclipse spectrometer. Ln³⁺ luminescence lifetimes were measured using the Varian Cary Eclipse spectrometer. Quantum yields were determined using the Fluorolog spectrometer by a relative method with quinine sulphate in 0.5 M H₂SO₄ as standard^{80,81}. Estimated experimental error for the quantum yield determination is ~10 %.

X-Ray diffraction. Single-crystal X-ray data were collected at 150 (2) K on a Rigaku XCalibur S CCD diffractometer equipped with a low temperature system and intensity data were collected using graphite-

monochromated Mo K α radiation ($\lambda = 0.71073 \text{ \AA}$). The data integration and reduction were processed with CrysAlis software (CrysAlisPro Software system, version 1.171.37.35, Agilent Technologies UK Ltd, Oxford). An analytical absorption correction was applied (Abspack, a part of the CrysAlisPro Software system, version 1.171.37.35, Agilent Technologies UK Ltd, Oxford). The structures were solved by direct methods using ShelXT software⁸² and were refined on F2 by the full-matrix least-squares technique using the SHELXL-2014 program package⁸³ in Olex2 environment.⁸⁴ Non-hydrogen atoms were refined anisotropically. Hydrogen atoms were found by Fourier transform and refined isotropically for **1**·NaBr and fixed in ideal position and refined with a riding model for ([Tb(L1)]Na(H₂O)₃)₂.

Compound 1·NaBr. To a solution of [1,4,7-*tris*(methoxycarbonylmethyl)]-1,4,7,10-tetraazacyclododecane hydrobromide⁷⁰ (2.62 g, 5.6 mmol) in CH₃CN (55 mL), was added Na₂CO₃ (2.28 g, 21.5 mmol) and then a solution of methyl 4-iodo-6-(((methylsulfonyl)oxy)methyl)picolinate⁴⁸ (1.59 g, 4.3 mmol) in CH₃CN (30 mL). The mixture was heated at reflux for 22 h, then cooled to room temperature and filtrated. The filtrate was evaporated under reduced pressure and the residue was triturated in Ethyl acetate to give **1**·NaBr as a white powder (3.29 g, 99 %). ¹H NMR (400 MHz, CDCl₃): $\delta = 8.33$ (d, $J = 1.4$ Hz, 1H), 7.91 (d, $J = 1.4$ Hz, 1H), 3.96 (s, 3H), 3.76 (s, 3H), 3.62, (s, 6H), 3.37-2.26 (m, 24H) ppm; ¹³C NMR (100 MHz, CDCl₃): δ (ppm) = 173.8, 172.7, 164.4, 160.0, 147.8, 136.7, 133.0, 107.9, 58.9, 55.4, 55.2, 53.2, 52.2, 52.1, 50.6 ppm; LRMS (ESI+): monoisotopic $m/z = 686.3$ [M+Na]⁺, 702.3 [M+K]⁺ (calculated monoisotopic $m/z = 686.17$ [M+Na]⁺, 702.14 [M+K]⁺ for M = C₂₅H₃₈IN₅O₈); HRMS (ESI+): monoisotopic $m/z = 664.1827$ (calculated monoisotopic $m/z = 664.1838$ [M+H]⁺ for M = C₂₅H₃₈IN₅O₈).

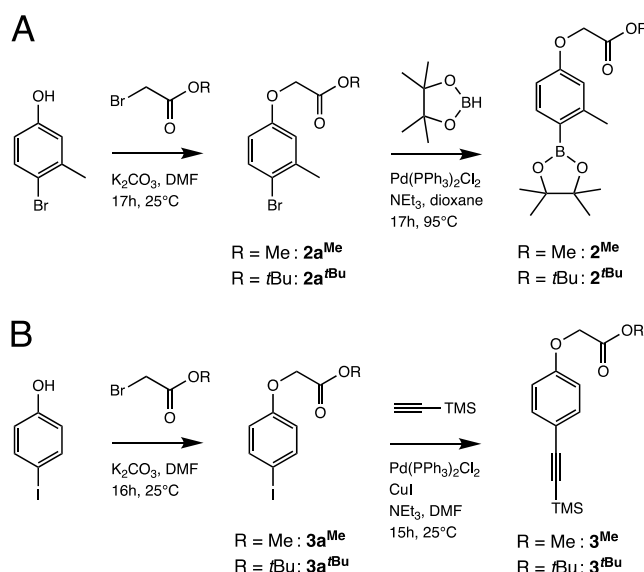


Figure 7. Pathways for the synthesis of (A) **2^{Me}** and **2^{tBu}** and (B) **3^{Me}** and **3^{tBu}**.

Methyl 2-(4-bromo-3-methylphenoxy)acetate (2^{Me}). To a solution of 4-bromo-3-methylphenol (1.0 g, 5.4 mmol) in DMF (10 mL) was added K₂CO₃ (2.2 g, 16 mmol) and methyl bromoacetate (610 μ L, 6.4 mmol). The mixture was stirred at room temperature for 17 h and then filtrated. The solvent was removed under reduced pressure. The oily residue was dissolved in CH₂Cl₂ and washed with water. The organic layer was dried over Na₂SO₄ and evaporated under reduced pressure to give **2^{Me}** as a colorless oil (1.28 g, 92 %) that could be used without further purification. ¹H NMR (400 MHz, CDCl₃): $\delta = 7.39$ (d, $J = 8.7$ Hz, 1H), 6.79 (d, $J = 3.0$ Hz, 2H), 6.58 (dd, $J = 3.0$ and 8.7 Hz, 1H), 4.57 (s, 2H), 3.77 (s, 3H), 2.33 (s, 3H) ppm; ¹³C NMR (100 MHz, CDCl₃): $\delta = 169.1, 157.0, 139.1, 132.9, 117.4, 116.6, 113.5, 65.3, 52.3, 23.1$ ppm.

Methyl 2-(3-methyl-4-(4,4,5,5-tetramethyl-1,3,2-dioxaborolan-2-yl)phenoxy)acetate (2^{Me}). To a degassed solution of **2^{Me}** (800 mg, 3.1 mmol) and *bis*(triphenylphosphine)palladium(II) dichloride (217 mg,

0.31 mmol) in dioxane (10 mL) was added under an inert atmosphere 4,4,5,5-tetramethyl-1,3,2-dioxaborane (1.4 mL, 9.3 mmol) and triethylamine (2.6 mL, 18.5 mmol). The mixture was heated at 95°C for 17 h. Solvents were removed under reduced pressure. The oily residue was dissolved in Ethyl acetate and washed with saturated NaHCO₃ and water. The organic layer was dried over Na₂SO₄ and the solvent was removed under reduced pressure to give a dark oil. The crude product was purified by flash chromatography (silica gel, CH₂Cl₂) to give **2^{Me}** as a yellow solid (773 mg, 82 %). ¹H NMR (400 MHz, CDCl₃): δ = 7.71 (d, *J* = 8.3 Hz, 1H), 6.72 (d, *J* = 2.5 Hz, 1H), 6.68 (dd, *J* = 2.5 and 8.3 Hz, 1H), 4.64 (s, 2H), 3.79 (3H), 2.51 (s, 3H), 1.32 (s, 12H) ppm; ¹³C NMR (100 MHz, CDCl₃): δ = 169.4, 159.9, 147.5, 138.0, 116.3, 110.6, 83.4, 65.1, 52.4, 25.0, 22.5 ppm; LRMS (ESI+): monoisotopic *m/z* = 329.3 [M+Na]⁺, 345.2 [M+K]⁺, 650.8 [2M+K]⁺ (calculated monoisotopic *m/z* = 329.15 [M+Na]⁺, 345.13 [M+K]⁺, 651.29 [2M+H]⁺ for M = C₁₆H₂₃BO₅).

tert-Butyl 2-(4-bromo-3-methylphenoxy)acetate (2^{Bu}). To a solution of 4-bromo-3-methylphenol (2.0 g, 10.7 mmol) in DMF (20 mL) was added K₂CO₃ (4.44 g, 32.1 mmol) and *tert*-butyl bromoacetate (1.9 mL, 12.8 mmol). The mixture was stirred at room temperature for 17 h and then filtrated. Solvents were removed under reduced pressure. The oily residue was dissolved in CH₂Cl₂ and washed with water. The organic layer was dried over Na₂SO₄ and evaporated under reduced pressure to give **2^{Bu}** as a colorless oil (3.12 g, 97 %) that could be used without further purification. ¹H NMR (400 MHz, CDCl₃): δ = 7.38 (d, *J* = 8.7 Hz, 1H), 6.79 (d, *J* = 2.9 Hz, 1H), 6.59 (dd, *J* = 2.9 and 8.7 Hz, 1H), 4.47 (s, 2H), 2.34 (s, 3H), 1.48 (s, 9H) ppm; ¹³C NMR (100 MHz, CDCl₃): δ = 167.8, 157.2, 139.0, 132.9, 117.4, 116.4, 113.5, 82.5, 65.8, 28.1, 23.2 ppm; LRMS (ESI+): monoisotopic *m/z* = 323.0 [M+Na]⁺, 339.0 [M+K]⁺ (calculated monoisotopic *m/z* = 323.03 [M+Na]⁺, 339.00 [M+K]⁺ for M = C₁₃H₁₇BrO₃).

tert-Butyl 2-(3-methyl-4-(4,4,5,5-tetramethyl-1,3,2-dioxaborolan-2-yl)phenoxy)acetate (2^{Bu}). To a degassed solution of **2^{Bu}** (750 mg, 2.5 mmol) and *bis*(triphenylphosphine)palladium(II) dichloride (175 mg, 0.2 mmol) in dioxane (10 mL) was added under an inert atmosphere 4,4,5,5-tetramethyl-1,3,2-dioxaborane (1.1 mL, 7.5 mmol) and triethylamine (2.1 mL, 15 mmol). The mixture was heated at 95°C for 17 h. Solvents were removed under reduced pressure and the residue was dissolved in Ethyl acetate and washed with saturated NaHCO₃ and brine. The organic layer was dried over Na₂SO₄ and the solvent was removed under reduced pressure to give a dark oil. The crude product was purified by flash chromatography (silica gel, CH₂Cl₂) to give **2^{Bu}** a yellow oil (720 mg, 83 %) that crystalizes after a few days. ¹H NMR (400 MHz, CDCl₃): δ = 7.71 (d, *J* = 8.2 Hz, 1H), 6.71 (d, *J* = 2.5 Hz, 1H), 6.67 (dd, *J* = 8.0 Hz, *J* = 2.3 Hz, 1H), 4.51 (s, 2H), 2.51 (s, 3H), 1.48 (s, 9H), 1.32 (s, 12H) ppm; ¹³C NMR (100 MHz, CDCl₃): δ = 168.1, 160.1, 147.4, 137.9, 116.3, 110.7, 83.3, 82.4, 65.5, 28.2, 25.0, 22.5 ppm; LRMS (ESI+): monoisotopic *m/z* = 371.2 [M+Na]⁺, 387.2 [M+K]⁺ (calculated monoisotopic *m/z* = 371.20 [M+Na]⁺, 387.17 [M+K]⁺ for M = C₁₉H₂₉BO₅).

Methyl 2-(4-iodophenoxy)acetate (3^{Me}). To a solution of 4-iodophenol (1.0 g, 4.55 mmol) in DMF (10 mL) was added potassium carbonate (1.88 g, 13.6 mmol) and methyl bromoacetate (515 μL, 5.4 mmol). The mixture was stirred at room temperature for 16 h and then filtrated. The solvent was removed under reduced pressure. The oily residue was dissolved in CH₂Cl₂ and washed with water. The organic layer was dried over Na₂SO₄ and the solvent was removed under reduced pressure to give **3^{Me}** as an oil (1.34 g, 100 %) that crystalizes after a few days. ¹H NMR (400 MHz, CDCl₃): δ = 7.56 (d, *J* = 8.5 Hz, 2H), 6.68 (d, *J* = 8.5 Hz, 2H), 4.60 (s, 2H), 3.80 (s, 3H) ppm; ¹³C NMR (100 MHz, CDCl₃): δ = 169.1, 157.8, 138.5, 117.1, 84.3, 65.4, 52.5 ppm (NMR data in agreement with Knutsson et al.⁸⁵); LRMS (ESI+): monoisotopic *m/z* = 315.0 [M+Na]⁺, 330.9 [M+K]⁺ (calculated monoisotopic *m/z* = 314.95 [M+Na]⁺, 330.92 [M+K]⁺ for M = C₉H₉IO₃).

Methyl 2-(4-((trimethylsilyl)ethynyl)phenoxy)acetate (3^{Me}). To a degassed solution of **3^{Me}** (800 mg, 2.74 mmol) and triethylamine (1.2 mL, 8.6 mmol) in DMF (1.2 mL) was added under an inert atmosphere *bis*(triphenylphosphine)palladium(II) dichloride (77 mg, 0.11 mmol), copper iodide (105 mg, 0.55 mmol) and ethynyltrimethylsilane (1.35 mL, 9.6 mmol). The mixture was stirred at room temperature for 15 h. Solvents were removed under reduced pressure. The residue was dissolved in CH₂Cl₂ and washed with saturated NH₄Cl and

water. The organic layer was dried over Na₂SO₄ and the solvent was removed under reduced pressure to give a dark oil. The crude product was purified by flash chromatography (silica gel, CH₂Cl₂) to give **3^{Me}** as brown crystals (683 mg, 95 %). ¹H NMR (400 MHz, CDCl₃): δ = 7.40 (d, *J* = 8.5 Hz, 2H), 6.82 (d, *J* = 8.6 Hz, 2H), 4.63 (s, 2H), 3.80 (s, 3H), 0.23 (s, 9H) ppm; ¹³C NMR (100 MHz, CDCl₃): δ = 169.1, 158.0, 133.7, 116.7, 114.6, 104.9, 93.1, 65.4, 52.5, 0.16 ppm; LRMS (ESI+): monoisotopic *m/z* = 285.2 [M+Na]⁺, 301.1 [M+K]⁺ (calculated monoisotopic *m/z* = 285.09 [M+Na]⁺, 301.07 [M+K]⁺ for M = C₁₄H₁₈O₃Si).

tert-Butyl 2-(4-iodophenoxy)acetate (3a^{tBu}). To a solution of 4-iodophenol (3.0 g, 13.6 mmol) in DMF (30 mL) was added potassium carbonate (10 g, 106 mmol), and *tert*-butyl bromoacetate (6 mL, 40.5 mmol). The mixture was stirred at room temperature for 16 h and then filtrated. The solvent was removed under reduced pressure. The oily residue was dissolved in CH₂Cl₂ and washed with water then brine. The organic layer was dried over Na₂SO₄ and the solvent removed under reduced pressure. The residue was purified by flash chromatography (silica gel, CH₂Cl₂) to give **3a^{tBu}** as a pale red liquid (3.43 g, 75 %). ¹H NMR (400 MHz, CDCl₃): δ = 7.51 (d, *J* = 9.0 Hz, 2H), 6.63 (d, *J* = 9.0 Hz, 2H), 4.44 (s, 2H), 1.45 (s, 9H) ppm; ¹³C NMR (100 MHz, CDCl₃): δ = 167.6, 157.8, 138.3, 117.0, 83.8, 82.6, 65.7, 28.0 ppm; LRMS (ESI+): monoisotopic *m/z* = 357.0 [M+Na]⁺, 373.0 [M+K]⁺ (calculated monoisotopic *m/z* = 357.00 [M+Na]⁺, 372.97 [M+K]⁺ for M = C₁₂H₁₅IO₃).

tert-Butyl 2-(4-((trimethylsilyl)ethynyl)phenoxy)acetate (3^{tBu}). To a degassed solution of **3a^{tBu}** (1.0 g, 3.0 mmol) and triethylamine (1.3 mL, 9.3 mmol) in DMF (1.3 mL) was added under an inert atmosphere *bis*(triphenylphosphine)palladium(II) dichloride (84 mg, 0.12 mmol), copper iodide (114 mg, 0.6 mmol) and ethynyltrimethylsilane (1.5 mL, 10.5 mmol). The mixture was stirred at room temperature for 15 h. Solvents were removed under reduced pressure. The residue was dissolved in CH₂Cl₂ and washed with saturated NH₄Cl and water. The organic layer was dried over Na₂SO₄ and the solvent was removed under reduced pressure to give a dark oil. The crude product was purified by flash chromatography (silica gel, Cyclohexane/Ethyl acetate 95:5) to give **3^{tBu}** as brown crystals (900 mg, 99 %). ¹H NMR (400 MHz, CDCl₃): δ = 7.39 (d, *J* = 9.0 Hz, 2H), 6.80 (d, *J* = 9.0 Hz, 2H), 4.50 (s, 2H), 1.47 (s, 9H), 0.23 (s, 9H) ppm; ¹³C NMR (100 MHz, CDCl₃): δ = 167.8, 158.2, 133.6, 116.3, 114.6, 105.0, 92.9, 82.7, 65.8, 28.1, 0.16 ppm.

L1. To a degassed solution of **1**·NaBr (100 mg, 0.131 mmol) and **2^{Me}** (37.5 mg, 0.122 mmol) in DMF (1.25 mL) was added *tetrakis*(triphenylphosphine)palladium(0) (14 mg, 0.012 mmol) and cesium fluoride (56 mg, 0.37 mmol). The mixture was stirred at 90°C for 17 h and then the solvent was removed under reduced pressure. The oily residue was dissolved in CH₂Cl₂ and washed with water. The organic layer was dried over Na₂SO₄ and evaporated under reduced pressure. Water (16 mL) was added to the crude and the suspension was sonicated for 20 min and centrifuged. The supernatant was lyophilized to give the pentamethyl ester **L1(Me)₅** as a yellow oil (102 mg), which was used without further purification. It was dissolved in 1M NaOH (4 mL) and stirred at rt. The reaction was completed after 15 min as monitored by HPLC. The pH was adjusted to 4 by addition of 1 M HCl (4 mL). The solution was purified on HPLC to give **L1**·3TFA as a yellow solid (72 mg, 60 %) after lyophilization. **L1**: ¹H NMR (400 MHz, D₂O, 353 K): δ = 8.11 (d, *J* = 1.5 Hz, 1H), 7.82 (d, *J* = 1.5 Hz, 1H), 7.28 (d, *J* = 8.4 Hz, 1H), 6.95 (d, *J* = 2.7 Hz, 1H), 6.92 (dd, *J* = 2.7 and 8.4 Hz, 1H), 4.76 (s, 2H), 4.49 (s, 2H), 3.84 (s, 2H), 3.62 (s, 4H), 3.43-3.18 (m, 16H), 2.24 (s, 3H) ppm; ¹³C NMR (100 MHz, D₂O, 353 K): δ = 173.3, 172.1, 171.0, 166.8, 158.8, 155.2, 151.3, 148.0, 138.5, 131.8, 131.3, 130.0, 126.8, 117.7, 113.3, 65.7, 57.8, 55.1, 54.5, 51.1, 50.8, 50.2, 50.1, 20.1 ppm; LRMS (ESI+): monoisotopic *m/z* = 646.4 [M+H]⁺, 668.4 [M+Na]⁺ (calculated monoisotopic *m/z* = 646.27 [M+H]⁺, 668.25 [M+Na]⁺ for M = C₃₀H₃₉N₅O₁₁); HRMS (ESI+): *m/z* = 646.2701 (calculated *m/z* = 646.2719 [M+H]⁺ for M = C₃₀H₃₉N₅O₁₁).

[Tb(L1)](Et₃NH). TbCl₃ (17.7 mg, 47 μmol) was added to a solution of **L1**·3TFA (27.8 mg, 28 μmol) in water (5 mL) and the pH was slowly raised to 9 by adding aliquots of triethylamine. The mixture was stirred at rt for 17 h. The reaction mixture was centrifuged and the supernatant evaporated under reduced pressure. Acetone was added and the suspension was sonicated and then centrifuged. The precipitate was collected and washed twice with acetone to give a white powder (21 mg, 85 %). HPLC (anal.) *t_R* = 6.5 min (method B); LRMS (ESI-):

monoisotopic $m/z = 800.2$ [M-H]⁻ (calculated monoisotopic $m/z = 800.16$ [M-H]⁻ for M = C₃₀H₃₆N₅O₁₁Tb); HRMS (ESI⁻): $m/z = 800.1586$ (calculated $m/z = 800.1592$ [M+H]⁻ for M = C₃₀H₃₆N₅O₁₁Tb).

[Eu(L1)](Et₃NH). This compound was obtained following the procedure described above for **[Tb(L1)](Et₃NH)** with EuCl₃ as a lanthanide salt. HPLC (anal.) $t_R = 6.6$ min (method B); LRMS (ESI⁻): monoisotopic $m/z = 794.2$ [M-H]⁻ (calculated monoisotopic $m/z = 794.15$ [M-H]⁻ for M = C₃₀H₃₆N₅O₁₁Eu); HRMS (ESI⁻): $m/z = 794.1548$ (calculated $m/z = 794.1551$ [M+H]⁻ for M = C₃₀H₃₆EuN₅O₁₁).

[Dy(L1)](Et₃NH). This compound was obtained following the procedure described above for **[Tb(L1)](Et₃NH)** with DyCl₃ as a lanthanide salt. HPLC (anal.) $t_R = 6.4$ min (method B); LRMS (ESI⁻): monoisotopic $m/z = 805.2$ [M-H]⁻ (calculated monoisotopic $m/z = 805.16$ [M-H]⁻ for M = C₃₀H₃₆N₅O₁₁Dy); HRMS (ESI⁻): $m/z = 805.1640$ (calculated $m/z = 805.1630$ [M+H]⁻ for M = C₃₀H₃₆DyN₅O₁₁).

L2. To a degassed solution of **1**·NaBr (100 mg, 0.131 mmol) and **3^{Me}** (29 mg, 0.111 mmol) in DMF (1.1 mL) was added triethylamine (425 μL, 3.05 mmol), *bis*(triphenylphosphine)palladium(II) dichloride (8 mg, 0.011 mmol) and tetrabutylammonium fluoride 1M in THF (130 μL, 0.130 mmol). The mixture was stirred at 90°C for 17 h. Solvents were removed under reduced pressure. The oily residue was dissolved in CH₂Cl₂ and washed with water. The organic layer was dried over Na₂SO₄ and evaporated under reduced pressure. Water (16 mL) was added to the crude and the suspension was sonicated for 20 min, then centrifuged. The supernatant was lyophilized to give the penta-methyl ester **L2(Me)₅** as a brown oil (99 mg), which used without further purification. It was dissolved in 1 M NaOH (4 mL) and stirred at rt. The reaction was completed in 15 min as monitored by HPLC. The pH was adjusted to 4 by addition of 1 M HCl (4 mL). The solution was purified by HPLC to give **L2**·3TFA as a yellow/orange solid (51 mg, 47 %) once lyophilized. ¹H NMR (400 MHz, D₂O, 353 K): δ = 8.02 (d, *J* = 1.4 Hz, 1H), 7.73 (d, *J* = 1.4 Hz, 1H), 7.46 (d, *J* = 9.0 Hz, 2H), 6.89 (d, *J* = 9.0 Hz, 2H), 4.66 (s, 2H), 4.25 (s, 2H), 3.67 (s, 2H), 3.55 (s, 4H), 3.31-3.08 (m, 16H) ppm; ¹³C NMR (100 MHz, D₂O, 353 K): δ = 173.1, 172.0, 171.4, 166.8, 159.4, 152.5, 148.4, 136.6, 134.7, 130.6, 127.7, 115.8, 114.8, 98.5, 85.8, 65.7, 57.8, 55.2, 54.6, 50.9, 50.7, 50.4, 50.2 ppm; LRMS (ESI⁺): monoisotopic $m/z = 656.4$ [M+H]⁺ (calculated monoisotopic $m/z = 656.26$ [M+H]⁺ for M = C₃₁H₃₇N₅O₁₁); HRMS (ESI⁺): $m/z = 656.2599$ (calculated $m/z = 656.2562$ [M+H]⁺ for M = C₃₁H₃₇N₅O₁₁).

[Eu(L2)](Et₃NH). To a solution of **L2**·3TFA (30 mg, 30 μmol) in water (5 mL) was added triethylamine to adjust the pH at 9. EuCl₃ (18.4 mg, 50 μmol) was added and the pH was adjusted to 9 by subsequent addition of triethylamine. The mixture was stirred at r.t for 17 h and centrifuged. The supernatant was evaporated under reduced pressure and acetone was added to precipitate the complex. The suspension was sonicated then centrifuged. The precipitate was washed twice with acetone to give **[Eu(L2)](Et₃NH)** a white powder (22 mg, 89 %). HPLC (anal.) $t_R = 7.4$ min (method B); LRMS (ESI⁻): monoisotopic $m/z = 803.8$ [M-H]⁻ (calculated monoisotopic $m/z = 804.14$ [M-H]⁻ for M = C₃₁H₃₄EuN₅O₁₁); HRMS (ESI⁻): $m/z = 804.1383$ (calculated $m/z = 804.1394$ [M+H]⁻ for M = C₃₁H₃₄N₅O₁₁Eu).

[Sm(L2)](Et₃NH). This compound was obtained following the procedure described above for **[Eu(L2)](Et₃NH)** with Sm(NO₃)₃ as a lanthanide salt. HPLC (anal.) $t_R = 7.5$ min (method B); LRMS (ESI⁻): monoisotopic $m/z = 803.2$ [M-H]⁻ (calculated monoisotopic $m/z = 803.14$ [M-H]⁻ for M = C₃₁H₃₄N₅O₁₁Sm); HRMS(ESI⁻): $m/z = 803.1364$ (calculated $m/z = 803.1379$ [M+H]⁻ for M = C₃₁H₃₄N₅O₁₁Sm).

L1(Me)₄. To a degassed solution of **1**·NaBr (100 mg, 0.131 mmol) and **2^{tBu}** (41 mg, 0.123 mmol) in DMF (1.25 mL) was added *tetrakis*(triphenylphosphine)palladium(0) (14 mg, 0.012 mmol) and cesium fluoride (56 mg, 0.37 mmol). The mixture was stirred at 90°C for 17 h and then the solvent was removed under reduced pressure. The oily residue was dissolved in CH₂Cl₂ and washed with water. The organic layer was dried over Na₂SO₄ and evaporated under reduced pressure. Water (16 mL) was added to the crude. The suspension was sonicated for 20 min and centrifuged. The supernatant was collected and lyophilized to give **L1(Me)₄(tBu)** as a brown oil (117 mg), which was identified by LC/MS but could not be characterized in depth due to the instability of the *tert*-butyl ester. It was used without further purification. Removal of the *t*Bu protecting group was performed in TFA

(5 mL) at rt for 2 h. TFA was evaporated under reduced pressure and the crude was dissolved in water and purified on HPLC to give **L1(Me)₄-3TFA** as a slightly yellow oil (52.6 mg, 41 %) after lyophilization. ¹H NMR (400 MHz, D₂O, 353 K): δ = 8.06 (d, *J* = 1.5 Hz, 1H), 7.83 (d, *J* = 1.5 Hz, 1H), 7.21 (d, *J* = 8.5 Hz, 1H), 6.95 (d, *J* = 2.7 Hz, 1H), 6.90 (dd, *J* = 2.7 and 8.5 Hz, 1H), 4.75 (s, 2H), 4.58 (s, 2H), 4.06 (s, 2H), 4.01 (s, 3H), 3.70 (s, 3H), 3.59 (s, 4H), 3.48 (s, 6H) 3.80-2.98 (m, 16H), 2.23 (s, 3H) ppm; ¹³C NMR (100 MHz, D₂O, 353 K): δ = 173.1, 172.5, 168.7, 166.8, 158.7, 153.1, 152.5, 148.0, 138.2, 131.5, 131.4, 129.7, 126.5, 117.7, 113.3, 65.7, 58.9, 54.9, 54.0, 53.2, 53.0, 52.9, 52.3, 52.2, 49.6, 49.1, 20.1 ppm; LRMS (ESI⁺): monoisotopic *m/z* = 702.4 [M+H]⁺, 724.4 [M+Na]⁺, 740.3 [M+K]⁺ (calculated monoisotopic *m/z* = 702.33 [M+H]⁺, 724.32 [M+Na]⁺, 740.29 [M+K]⁺ for M = C₃₄H₄₇N₅O₁₁); HRMS (ESI⁺): *m/z* = 702.3328 (calculated *m/z* = 702.3345 [M+H]⁺ for M = C₃₄H₄₇N₅O₁₁).

L2(Me)₄. To a degassed solution of **1**·NaBr (100 mg, 0.131 mmol) and **3^{tBu}** (33 mg, 0.108 mmol) in DMF (1.1 mL) was added triethylamine (425 μL, 3.05 mmol), *bis*(triphenylphosphine)palladium(II) dichloride (8 mg, 11.4 μmol) and tetrabutylammonium fluoride 1M in THF (130 μL, 130 μmol). The mixture was stirred at 90°C for 17 h. Solvents were removed under reduced pressure. The oily residue was dissolved in CH₂Cl₂ and washed water. The organic layer was dried over Na₂SO₄ and evaporated under reduced pressure. Water (16 mL) was added to the crude and the suspension was sonicated for 20 min, then centrifuged. The supernatant was lyophilized to give **L2(Me)₄(*t*Bu)** as a brown oil (121 mg), which was identified by LC/MS but could not be characterized in depth due to the instability of the *tert*-butyl ester. It was used without further purification. Removal of the *t*Bu protecting group was performed in TFA (5 mL) at rt for 2 h. TFA was evaporated under reduced pressure and the crude was dissolved in water and purified on HPLC to give **L2(Me)₄-3TFA** as a brown oil (38.6 mg, 34 %) after lyophilization. ¹H NMR (400 MHz, D₂O, 353 K): δ = 8.16 (d, *J* = 1.0 Hz, 1H), 7.87 (d, *J* = 1.0 Hz, 1H), 7.54 (d, *J* = 8.8 Hz, 2H), 7.02 (d, *J* = 8.8 Hz, 2H), 4.76 (s, 2H), 4.45 (s, 2H), 4.03 (s, 3H), 4.01 (s, 2H), 3.74 (s, 3H), 3.66 (s, 4H), 3.61 (s, 6H), 3.54-3.02 (m, 16H) ppm; ¹³C NMR (100 MHz, D₂O, 353 K): δ (ppm) = 173.3, 172.0, 169.5, 166.4, 159.5, 148.2, 135.3, 134.5, 134.4, 130.9, 127.4, 115.9, 114.7, 97.4, 85.5, 65.9, 58.5, 54.8, 54.1, 53.9, 53.3, 53.2, 52.0, 51.8, 50.0, 49.6 ppm; LRMS (ESI⁺): monoisotopic *m/z* = 712.6 [M+H]⁺, 734.6 [M+Na]⁺, 750.6 [M+K]⁺ (calculated monoisotopic *m/z* = 712.32 [M+H]⁺, 734.30 [M+Na]⁺, 750.27 [M+K]⁺ for M = C₃₅H₄₅N₅O₁₁); HRMS (ESI⁺): *m/z* = 712.3174 (calculated *m/z* = 712.3188 [M+H]⁺ for M = C₃₅H₄₅N₅O₁₁).

Peptide sequences. **TP2[L1]:** PLIYLRLLRGQFK(L1)-NH₂; **TP2[L1(Me)₄]:** PLIYLRLLRGQFK(L1(Me)₄)-NH₂; **TP2[Tb(L1)]:** PLIYLRLLRGQFK(Tb(L1))-NH₂; **TP2[L2(Me)₄]:** PLIYLRLLRGQFK(L2(Me)₄)-NH₂; **TP2[Eu(L2)]:** PLIYLRLLRGQFK(Eu(L2))-NH₂; **ZF⁵⁻³[L1(Me)₄]:** Ac-K(L1(Me)₄)AFSCNVC GKAFVLSRHLNRHLRVHRRAT-NH₂; **ZF⁵⁻³[Tb(L1)]:** Ac-K(Tb(L1))AFSCNVC GKAFVLSRHLNRHLRVHRRAT-NH₂

Peptide elongation: Peptide elongation was performed using standard SPPS procedure using Fmoc/*t*Bu chemistry on an automated peptide synthesizer (CEM Liberty1 Microwave Peptide Synthesizer) under microwave irradiation following standard protocols established by CEM⁸⁶ with double coupling and capping. Fmoc removal was performed using 20% piperidine in DMF. Couplings were performed using 4-fold molar excess of Fmoc-L-amino acid (0.2 M in DMF), 3.6-fold molar excess of HCTU (0.45 M in DMF) and 8-fold molar excess of *N,N*-diisopropylethylamine (DIEA; 2 M in *N*-methyl-2-pyrrolidone). A capping step was performed after each coupling with acetic anhydride (Ac₂O; 2% in DMF) and DIEA (2 M in *N*-methyl-2-pyrrolidone).

TP2[L1(Me)₄]: The peptide was synthesized on Rink-PEG-PS resin (Nova PEG Rink Amide, 0.09 mmol, 0.37 mmol/g). The first amino acid was attached by single manual coupling (30 min) using 3-fold excess of Fmoc-Lys(Alloc)-OH, 2.7-fold excess of HCTU and 6-fold excess of DIEA in DMF followed by a capping step using Ac₂O/pyridine/DMF (1:2:7 v/v/v, 10 mL, 5 min). Fmoc removal was performed by three successive treatments with 20% piperidine in DMF (8 mL) for 3 min. Then, automated peptide elongation was performed as described above. After the final Fmoc removal, the N-terminus was protected by a Boc group by reaction with di-*tert*-butyl dicarbonate (0.11 mmol, 1.2 eq, 24 mg) in CH₂Cl₂ overnight. Removal of the Alloc protecting group was performed by adding a solution of Pd(PPh₃)₄ (0.045 mmol, 0.5 eq., 55 mg) and phenylsilane (2.2 mmol, 25 eq.,

0.27 mL) in degassed CH₂Cl₂ (10 mL) for 1 h in the dark (twice).⁸⁷ The resin was then washed successively with CH₂Cl₂ (2×2 min), DMF (2×2 min), 1% H₂O in DMF (2×2 min), DMF (2×2 min), 1% DIEA in DMF (2×2 min), DMF (2×2 min), sodium diethyldithiocarbamate in DMF (0.12 M, 2×5 min) and DMF (2×2 min). The rest of the synthesis was performed on the 20 μmol scale. **L1(Me)₄** (0.03 mmol, 21 mg, 1.5 eq.) was coupled to the peptide with PyBOP (0.03 mmol, 16 mg, 1.5 eq.) and DIEA (0.12 mmol, 20 μL, 6 eq) in DMF (2 mL). Removal of acid-labile side chain protecting groups and resin cleavage were performed using TFA / H₂O / triisopropylsilane / thioanisole (92.5:2.5:2.5:2.5 v/v/v/v, 2 mL) for 2 h. The peptide was precipitated in cold Et₂O, centrifuged, washed twice with Et₂O, purified by HPLC and freeze-dried to give **TP2[L1(Me)₄]** (10 mg, 17% yield for the **TP2[L1(Me)₄]**·(TFA)₆ salt). HPLC (anal.): *t_R* = 9.0 min (method B); LRMS (ESI+): average *m/z* = 1150.7 (2+), 767.5 (3+), 575.9 (4+), 461.0 (5+) / calculated av. *m/z* = 1150.89 [M+2H]²⁺, 767.59 [M+3H]³⁺, 575.95 [M+4H]⁴⁺, 460.96 [M+5H]⁵⁺ for M = C₁₁₂H₁₇₅N₂₇O₂₅); deconvoluted mass found = 2299.5 / expected mass = 2299.76 (average isotopic composition).

TP2[L1]: Hydrolysis of methyl esters of **TP2[L1(Me)₄]** was performed by reacting the peptide (10 mg) in 0.1 M NaOH (10 mL) for 2 h. The pH was neutralized using 1 M HCl and the peptide was purified by HPLC to give **TP2[L1]** (7 mg, 70% yield for the **TP2[L1]**·(TFA)₆ salt). HPLC (anal.): *t_R* = 13.3 min (method A); LRMS (ESI+): average *m/z* = 1122.7 (2+), 748.6 (3+), 561.8 (4+), 449.7 (5+) / calculated av. *m/z* = 1122.83 [M+2H]²⁺, 748.89 [M+3H]³⁺, 561.92 [M+4H]⁴⁺, 449.74 [M+5H]⁵⁺ for M = C₁₀₈H₁₆₇N₂₇O₂₅); deconvoluted mass found = 2243.4 / expected mass = 2243.65 (average isotopic composition).

TP2[Tb(L1)]: Compound **TP2[L1]** (1.2 μmol, 3 mg) and TbCl₃·(H₂O)₆ (11 μmol, 4 mg, 10 eq.) were dissolved in H₂O (0.6 mL) and the pH was adjusted to 7.5 using aqueous NaOH. The solution was stirred overnight at rt. After HPLC purification and freeze-drying, **TP2[Tb(L1)]** was obtained as a white powder (95%). HPLC (anal.): *t_R* = 8.9 min (method B); LRMS (ESI+): average *m/z* = 1200.2 (2+), 800.6 (3+), 600.8 (4+) / calculated av. *m/z* = 1200.78 [M+2H]²⁺, 800.86 [M+3H]³⁺, 600.90 [M+4H]⁴⁺ for M = C₁₀₈H₁₆₄N₂₇O₂₅Tb); deconvoluted mass found = 2399.0 / expected mass = 2399.55 (average isotopic composition).

TP2[L2(Me)₄]: This compound was prepared following the procedure as described above for **TP2[L1(Me)₄]** up to Alloc removal. Then the synthesis was continued on the 10 μmol scale. **L2(Me)₄** (0.015 mmol, 11 mg, 1.5 eq.) was coupled to the peptide with PyBOP (0.025 mmol, 13 mg, 2.5 eq.) and DIEA (0.06 mmol, 10 μL, 6 eq) in DMF (2 mL). Removal of acid-labile side chain protecting groups and resin cleavage were performed using TFA/H₂O (97:3 v/v, 2 mL) containing dithiothreitol (60 mg) for 2 h. The peptide was precipitated in cold Et₂O, centrifuged, washed twice with Et₂O, purified by HPLC and freeze-dried to give **TP2[L2(Me)₄]** (4 mg, 14% yield for the **TP2[L2(Me)₄]**·(TFA)₆ salt). HPLC (anal.): *t_R* = 9.0 min (method B); LRMS (ESI+): average *m/z* = 1155.7 (2+), 770.8 (3+), 578.3 (4+), 462.9 (5+) / calculated av. *m/z* = 1155.88 [M+2H]²⁺, 770.93 [M+3H]³⁺, 578.45 [M+4H]⁴⁺, 462.96 [M+5H]⁵⁺ for M = C₁₁₃H₁₇₃N₂₇O₂₅); deconvoluted mass found = 2309.4 / expected mass = 2309.75 (average isotopic composition).

TP2[Eu(L2)]: Hydrolysis of methyl esters of **TP2[L2(Me)₄]** was performed by reacting the peptide in 0.5 M NaOH (1 mL) for 40 min. Complete formation of **TP2[L2]** was confirmed by LCMS analysis (HPLC (anal.): *t_R* = 8.6 min (method B); LRMS (ESI+): average *m/z* = 1127.7 (2+), 751.9 (3+), 564.4 (4+), 451.5 (5+) / calculated av. *m/z* = 1127.83 [M+2H]²⁺, 752.22 [M+3H]³⁺, 564.42 [M+4H]⁴⁺, 451.74 [M+5H]⁵⁺ for M = C₁₀₉H₁₆₅N₂₇O₂₅); deconvoluted mass found = 2253.3 / expected mass = 2253.65 (average isotopic composition)). The pH was neutralized using 1 M HCl and EuCl₃·(H₂O)₆ (15 μmol, 5.5 mg, 15 eq.) was added. The pH was adjusted to 7.5 using aqueous NaOH and the solution was stirred overnight at rt. After HPLC purification and freeze-drying, **TP2[Eu(L2)]** was obtained as a white powder (3 mg, 73% yield for the **TP2[L2(Me)₄]**·(TFA)₆ salt). HPLC (anal.): *t_R* = 8.9 min (method B); LRMS (ESI+): average *m/z* = 1202.0 (2+), 801.8 (3+), 601.7 (4+) / calculated av. *m/z* = 1202.30 [M+2H]²⁺, 801.87 [M+3H]³⁺, 601.65 [M+4H]⁴⁺ for M = C₁₀₉H₁₆₂N₂₇O₂₅Eu); deconvoluted mass found = 2402.3 / expected mass = 2402.59 (average isotopic composition).

ZF^{5.3}[L1(Me)₄]: The peptide was synthesized on Rink-PEG-PS resin (Nova PEG Rink Amide, 0.12 mmol, 0.37 mmol/g). The first amino acid was attached by single manual coupling (30 min) using 3-fold excess of Fmoc-Thr(*t*Bu)-OH, 3-fold excess of PyBOP and 6-fold excess of DIEA in DMF followed by a capping step using Ac₂O/pyridine/DMF (1:2:7 v/v/v, 10 mL, 5 min). Fmoc removal was performed by treatment with 20% piperidine in DMF (3×3 min). Then, automated peptide elongation was performed as described above. The last amino acid was introduced by double manual coupling (30 min) using 3-fold excess of Fmoc-Lys(Alloc)-OH, 3-fold excess of PyBOP and 6-fold excess of DIEA in DMF. After the final Fmoc removal (20% piperidine, 3×3 min), the N-terminus was acetylated using Ac₂O/pyridine/DMF (1:2:7 v/v/v, 10 mL, 5 min). Removal of the Alloc protecting group was performed by adding a solution of Pd(PPh₃)₄ (0.04 mmol, 0.33 eq., 37 mg) and phenylsilane (3.0 mmol, 25 eq., 0.37 mL) in degassed CH₂Cl₂ (10 mL) for 1 h in the dark (twice).⁸⁷ The resin was then washed successively with CH₂Cl₂ (2×2 min), DMF (2×2 min), 1% H₂O in DMF (2×2 min), DMF (2×2 min), 1% DIEA in DMF (2×2 min), DMF (2×2 min), sodium diethyldithiocarbamate in DMF (0.12 M, 2×5 min) and DMF (2×2 min). The rest of the synthesis was performed on the 20 μmol scale. **L1(Me)₄** (0.03 mmol, 21 mg, 1.5 eq.) was coupled to the peptide with PyBOP (0.03 mmol, 16 mg, 1.5 eq.) and DIEA (0.12 mmol, 20 μL, 6 eq) in DMF (2 mL). Removal of acid-labile side chain protecting groups and resin cleavage were performed using TFA / H₂O / triisopropylsilane / thioanisole (92.5:2.5:2.5:2.5 v/v/v/v, 2 mL) for 2 h. The peptide was precipitated in cold Et₂O, centrifuged, washed twice with Et₂O, purified by HPLC and freeze-dried to give **ZF^{5.3}[L1(Me)₄]** (5 mg, 5% yield for the **ZF^{5.3}[L1(Me)₄]**·(TFA)₁₂ salt). HPLC (anal.): *t_R* = 8.2 min (method b); LRMS (ESI+): average *m/z* = 1406.2 (3+), 1444.2 (3+), 1482.3 (3+), 1026.5 (4+), 1055.0 (4+), 1083.4 (4+), 821.4 (5+), 844.2 (5+), 684.7 (6+), 703.6 (6+), 587.0 (7+), 513.7 (8+) / calculated av. *m/z* = 1406.60 [M+TFA+3H]³⁺, 1444.61 [M+2TFA+3H]³⁺, 1482.62 [M+3TFA+3H]³⁺, 1026.70 [M+4H]⁴⁺, 1055.20 [M+TFA+4H]⁴⁺, 1083.71 [M+2TFA+4H]⁴⁺, 821.56 [M+5H]⁵⁺, 844.37 [M+TFA+5H]⁵⁺, 684.80 [M+6H]⁶⁺, 703.81 [M+TFA+6H]⁶⁺, 587.12 [M+7H]⁷⁺, 513.85 [M+8H]⁸⁺ for M = C₁₈₂H₂₉₀N₆₀O₄₅S₂; deconvoluted mass found = 4102.1 / expected mass = 4102.77 (average isotopic composition).

ZF^{5.3}[Tb(L1)]: Hydrolysis of methyl esters of **ZF^{5.3}[L1(Me)₄]** was performed by reacting the peptide in 0.3 M NaOH (1 mL) for 20 min. The pH was neutralized using 1 M HCl. The solution was eluted on Waters Oasis HLB 3cc (400mg) extraction cartridge to remove salts and the fraction containing the peptide was lyophilized. The peptide and TbCl₃·(H₂O)₆ (11 μmol, 4 mg, 12 eq.) were dissolved in H₂O (0.6 mL) and the pH was adjusted to 7.5 using aqueous NaOH. The solution was stirred overnight at rt. After HPLC purification and freeze-drying, **ZF^{5.3}[Tb(L1)]** was obtained as a white powder (3 mg, 58% yield for the **ZF^{5.3}[Tb(L1)]**·(TFA)₁₂ salt). HPLC (anal.): *t_R* = 7.9 min (method B); LRMS (ESI+): average *m/z* = 1401.6 (3+), 1439.7 (3+), 1051.4 (4+), 841.4 (5+), 701.4 (6+), 601.3 (7+) / calculated av. *m/z* = 1401.86 [M+3H]³⁺, 1439.87 [M+TFA+3H]³⁺, 1051.65 [M+4H]⁴⁺, 841.52 [M+5H]⁵⁺, 701.43 [M+6H]⁶⁺, 601.37 [M+7H]⁷⁺ for M = C₁₇₈H₂₇₉N₆₀O₄₅S₂Tb; deconvoluted mass found = 4201.9 / expected mass = 4202.56 (average isotopic composition).

Determination of the extinction coefficient of [Ln(L1)]⁻ and [Ln(L1)]⁻ complexes: A solution of ligand **L1** or **L2** was prepared by dissolving the ligand in HEPES buffer (10 mM, pH 7.5) and it titrated by a solution of TbCl₃ or EuCl₃ of known concentration with absorption monitoring (Figure S5 of Supporting Information).

1P time-gated microscopy. NIH3T3 mouse embryonic fibroblast cell line was grown in Dulbecco's modified eagle medium (DMEM, Sigma-Aldrich, D6546), supplemented with 10% fetal bovine serum (FBS, Sigma-Aldrich, F0804), 1% antibiotics (Pen Strep, Sigma-Aldrich, P4333), and 2 mM L-glutamine (Sigma-Aldrich, G7513) at 37°C and 5% CO₂. The cells were passaged with trypsin-EDTA 0.05%. Cells were seeded at 2×10⁵ cells/dish onto glass bottom petri dishes (CELLview Petri dishes 35×10 mm, Greiner Bio-One, 627860) and incubated at 37°C and 5% CO₂ overnight. The next day, the cells were washed with PBS (Thermo Fisher Scientific). **ZF^{5.3}[Tb(L1)]** was incubated at a concentration of 10 μM in PBS for 4 hours at 37°C and 5% CO₂. After incubation, the cells were washed twice with PBS and 1.5 mL of Opti-MEM I reduced serum medium (1×, Gibco, 11058-021) was added to the cell dish for observation under the microscope. Cell imaging was performed using a wide-field, inverted microscope (Olympus IX83), coupled with UV laser (337 nm, 300 Hz, MNL 330,

LTB Lasertechnik Berlin) for pulsed excitation and an intensified CCD camera (ICCD, PI-MAX4, Princeton Instruments) for time gated-detection. Laser power was significantly reduced by using neutral density filters (ND Filter OD 0.5: NDUVO5B, Thorlabs). The laser beam was redirected onto the sample with a 355 nm dichroic mirror (Di01-R355, Semrock Inc.). PL signals of the samples were collected with a high numerical aperture (NA = 1.35) immersion oil objective (UPLSAPO 60×O, Olympus) and detected using a 543 nm band-pass filter (FF01-543/20–25, Semrock Inc.). Acquisition settings in Winview software controlling the camera were fixed at a delay time of 100 μs, gate width of 3 ms, and intensifier gain of 50 V. DIC images were acquired with no delay time, a gate width of 300 ms, and an intensifier gain at 1 V.

2P confocal microscopy. HeLa cells were grown in in DMEM supplemented with 10% fetal bovine serum (v/v), and 2 mM L-glutamine at 37°C in a 5% CO₂ humidified atmosphere. HeLa cells were seeded at 3x10⁴ cells/well onto a 8-chamber Labtek-I coverglass system. After 24 h, cells were washed three times with PBS. Cells were incubated with ZF^{5.3}[Tb(L1)] (10 μM) in PBS at 37°C for 1 h. Then, cells were washed three times with PBS before adding fresh PBS (200 μL) for observation under microscope. Confocal 2P experiments were performed by using an LSM-DuoScan-Confocor3 NLO microscope (Carl Zeiss) composed of a LSM710 confocal module and an inverted motorized stand (AxioObserver) equipped with an on-stage cell incubator. Excitation was provided by a Ti:Sapphire femtosecond laser (Chameleon, Ultra II, Coherent) featuring chirp precompensation. The C-apochromat 40×/1.2 water-immersion objective was used throughout experiments. The pinhole was open during 2P acquisition in descanned detection mode. The spectral PMT detector (Quasar) or avalanche photodiodes were used to register the emission signal in each pixel of the confocal image. Temporal Sampling Lifetime Imaging Microscopy (TSLIM) was used to record luminescence lifetime decay in cells (single pulsed excitation with the 7.56 μs temporal resolution).⁴⁷

Acknowledgements

Authors acknowledge the Labex ARCANE, CBH-EUR-GS (ANR-17-EURE-0003), the Agence Nationale de la Recherche (ANR-18-CE06-0022), the Labex SynOrg (ANR-11-LABX-0029), the XL-Chem graduate school (ANR-18-EURE-0020), and the Région Normandie for financial support.

Supporting information available

HPLC chromatograms of complexes [Ln(L1)](Et₃NH) and [Ln(L2)](Et₃NH), HPLC chromatograms and LRMS spectra of conjugates, absorbance titration of L1 and L2 by LnCl₃ and crystallographic data for 1·NaBr and ([Tb(L1)]Na(H₂O)₃)₂, (PDF).

Accession Codes

CCDC 2212226-2212227 contains the supplementary crystallographic data for this paper. These data can be obtained free of charge via www.ccdc.cam.ac.uk/data_request/cif, or by emailing data_request@ccdc.cam.ac.uk, or by contacting The Cambridge Crystallographic Data Centre, 12 Union Road, Cambridge CB2 1EZ, UK; fax: +44 1223 336033.

References

- (1) Bünzli, J.-C. G.; Eliseeva, S. V. Basics of Lanthanide Photophysics. In *Lanthanide Luminescence*; Hänninen, P., Härmä, H., Eds.; Springer Series on Fluorescence; Springer Berlin Heidelberg, 2011; pp 1–45.
- (2) Eliseeva, S. V.; Bünzli, J.-C. G. Lanthanide Luminescence for Functional Materials and Bio-Sciences. *Chem. Soc. Rev.*

- 2010**, 39 (1), 189–227. <https://doi.org/10.1039/b905604c>.
- (3) Hildebrandt, N.; Wegner, K. D.; Algar, W. R. Luminescent Terbium Complexes: Superior Förster Resonance Energy Transfer Donors for Flexible and Sensitive Multiplexed Biosensing. *Coord. Chem. Rev.* **2014**, 273–274, 125–138. <https://doi.org/10.1016/j.ccr.2014.01.020>.
 - (4) Heffern, M. C.; Matosziuk, L. M.; Meade, T. J. Lanthanide Probes for Bioresponsive Imaging. *Chem. Rev.* **2014**, 114 (8), 4496–4539. <https://doi.org/10.1021/cr400477t>.
 - (5) Butler, S. J.; Delbianco, M.; Lamarque, L.; McMahon, B. K.; Neil, E. R.; Pal, R.; Parker, D.; Walton, J. W.; Zwier, J. M. EuroTracker® Dyes: Design, Synthesis, Structure and Photophysical Properties of Very Bright Europium Complexes and Their Use in Bioassays and Cellular Optical Imaging. *Dalton Trans.* **2015**, 44 (11), 4791–4803. <https://doi.org/10.1039/C4DT02785J>.
 - (6) Bünzli, J.-C. G. Lanthanide Light for Biology and Medical Diagnosis. *J. Lumin.* **2016**, 170, 866–878. <https://doi.org/10.1016/j.jlumin.2015.07.033>.
 - (7) Sy, M.; Nonat, A.; Hildebrandt, N.; Charbonnière, L. J. Lanthanide-Based Luminescence Biolabelling. *Chem. Commun.* **2016**, 52 (29), 5080–5095. <https://doi.org/10.1039/C6CC00922K>.
 - (8) Hewitt, S. H.; Butler, S. J. Application of Lanthanide Luminescence in Probing Enzyme Activity. *Chem. Commun.* **2018**, 54 (50), 6635–6647. <https://doi.org/10.1039/c8cc02824a>.
 - (9) Mathieu, E.; Sipos, A.; Demeyere, E.; Phipps, D.; Sakaveli, D.; Borbas, K. E. Lanthanide-Based Tools for the Investigation of Cellular Environments. *Chem. Commun.* **2018**, 54 (72), 10021–10035. <https://doi.org/10.1039/C8CC05271A>.
 - (10) Jin, G.-Q.; Ning, Y.; Geng, J.-X.; Jiang, Z.-F.; Wang, Y.; Zhang, J.-L. Joining the Journey to near Infrared (NIR) Imaging: The Emerging Role of Lanthanides in the Designing of Molecular Probes. *Inorg. Chem. Front.* **2020**, 7 (2), 289–299. <https://doi.org/10.1039/C9QI01132C>.
 - (11) Parker, D.; Fradgley, J. D.; Wong, K.-L. The Design of Responsive Luminescent Lanthanide Probes and Sensors. *Chem. Soc. Rev.* **2021**, 50 (14), 8193–8213. <https://doi.org/10.1039/D1CS00310K>.
 - (12) Lee, K.; Dzubeck, V.; Latshaw, L.; Schneider, J. P. De Novo Designed Peptidic Redox Potential Probe: Linking Sensitized Emission to Disulfide Bond Formation. *J. Am. Chem. Soc.* **2004**, 126 (42), 13616–13617. <https://doi.org/10.1021/ja047300r>.
 - (13) Isaac, M.; Denisov, S. A.; Roux, A.; Imbert, D.; Jonusauskas, G.; McClenaghan, N. D.; Sénèque, O. Lanthanide Luminescence Modulation by Cation– π Interaction in a Bioinspired Scaffold: Selective Detection of Copper(I). *Angew. Chem., Int. Ed.* **2015**, 54 (39), 11453–11456. <https://doi.org/10.1002/anie.201505733>.
 - (14) Raibaut, L.; Vasseur, W.; Shimberg, G. D.; Saint-Pierre, C.; Ravanat, J.-L.; Michel, S. L. J.; Sénèque, O. Design of a Synthetic Luminescent Probe from a Biomolecule Binding Domain: Selective Detection of AU-Rich MRNA Sequences. *Chem. Sci.* **2017**, 8 (2), 1658–1664. <https://doi.org/10.1039/C6SC04086A>.
 - (15) Isaac, M.; Raibaut, L.; Cepeda, C.; Roux, A.; Boturyn, D.; Eliseeva, S. V.; Petoud, S.; Sénèque, O. Luminescent Zinc Fingers: Zn-Responsive Neodymium Near-Infrared Emission in Water. *Chem.-Eur. J.* **2017**, 23 (46), 10992–10996. <https://doi.org/10.1002/chem.201703089>.
 - (16) Cepeda, C.; Raibaut, L.; Fremy, G.; Eliseeva, S. V.; Romieu, A.; Pecaut, J.; Boturyn, D.; Petoud, S.; Sénèque, O. Using Native Chemical Ligation for Site-Specific Synthesis of Hetero-Bis-Lanthanide Peptide Conjugates: Application to Ratiometric Visible or Near-Infrared Detection of Zn²⁺. *Chem.-Eur. J.* **2020**, 26 (59), 13476–13483. <https://doi.org/10.1002/chem.202002708>.
 - (17) Bhattacharya, K.; Bernasconi, L.; Picard, D. Luminescence Resonance Energy Transfer between Genetically Encoded Donor and Acceptor for Protein-Protein Interaction Studies in the Molecular Chaperone HSP70/HSP90 Complexes. *Sci. Rep.* **2018**, 8, 2801. <https://doi.org/10.1038/s41598-018-21210-6>.
 - (18) Falcone, E.; Gonzalez, P.; Lorusso, L.; Sénèque, O.; Faller, P.; Raibaut, L. A Terbium(III) Luminescent ATCUN-Based Peptide Sensor for Selective and Reversible Detection of Copper(II) in Biological Media. *Chem. Commun.* **2020**, 56 (35), 4797–4800. <https://doi.org/10.1039/d0cc01007c>.
 - (19) Kong, H.-K.; Chadbourne, F. L.; Law, G.-L.; Li, H.; Tam, H.-L.; Cobb, S. L.; Lau, C.-K.; Lee, C.-S.; Wong, K.-L. Two-Photon Induced Responsive f-f Emissive Detection of Cyclin A with a Europium-Chelating Peptide. *Chem. Commun.* **2011**, 47 (28), 8052–8054. <https://doi.org/10.1039/C1CC12811F>.
 - (20) Pazos, E.; Perez, M.; Gutierrez-de-Teran, H.; Orzaez, M.; Guevara, T.; Mascareñas, J. L.; Eugenio Vazquez, M. Rational Design of a Cyclin A Fluorescent Peptide Sensor. *Org. Biomol. Chem.* **2011**, 9 (22), 7629–7632. <https://doi.org/10.1039/c1ob06009k>.
 - (21) Pazos, E.; Jimenez-Balsa, A.; Mascareñas, J. L.; Vázquez, M. E. Sensing Coiled-Coil Proteins through Conformational Modulation of Energy Transfer Processes - Selective Detection of the Oncogenic Transcription Factor c-Jun. *Chem. Sci.* **2011**, 2 (10), 1984–1987. <https://doi.org/10.1039/c1sc00108f>.
 - (22) Pazos, E.; Golicnik, M.; Mascareñas, J. L.; Vázquez, M. E. Detection of Phosphorylation States by Intermolecular Sensitization of Lanthanide-Peptide Conjugates. *Chem. Commun.* **2012**, 48 (76), 9534–9536. <https://doi.org/10.1039/c2cc34958b>.
 - (23) Penas, C.; Pazos, E.; Mascareñas, J. L.; Vázquez, M. E. A Folding-Based Approach for the Luminescent Detection of a Short RNA Hairpin. *J. Am. Chem. Soc.* **2013**, 135 (10), 3812–3814. <https://doi.org/10.1021/ja400270a>.
 - (24) Penas, C.; Mascareñas, J. L.; Vázquez, M. E. Coupling the Folding of a β -Hairpin with Chelation-Enhanced Luminescence of Tb(III) and Eu(III) Ions for Specific Sensing of a Viral RNA. *Chem. Sci.* **2016**, 7 (4), 2674–2678. <https://doi.org/10.1039/C5SC04501K>.
 - (25) González-Vera, J. A.; Bouzada, D.; Bouclier, C.; Vázquez, M. E.; Morris, M. C. Lanthanide-Based Peptide Biosensor to Monitor CDK4/Cyclin D Kinase Activity. *Chem. Commun.* **2017**, 53 (45), 6109–6112. <https://doi.org/10.1039/C6CC09948C>.
 - (26) Maurel, D.; Comps-Agrar, L.; Brock, C.; Rives, M.-L.; Bourrier, E.; Ayoub, M. A.; Bazin, H.; Tinel, N.; Durroux, T.;

- Prézeau, L.; Trinquet, E.; Pin, J.-P. Cell-Surface Protein-Protein Interaction Analysis with Time-Resolved FRET and Snap-Tag Technologies: Application to GPCR Oligomerization. *Nat. Methods* **2008**, *5* (6), 561–567. <https://doi.org/10.1038/nmeth.1213>.
- (27) Zwier, J. M.; Bazin, H.; Lamarque, L.; Mathis, G. Luminescent Lanthanide Cryptates: From the Bench to the Bedside. *Inorg. Chem.* **2014**, *53* (4), 1854–1866. <https://doi.org/10.1021/ic402234k>.
- (28) Dantas de Araujo, A.; Wu, C.; Wu, K.-C.; Reid, R. C.; Durek, T.; Lim, J.; Fairlie, D. P. Europium-Labeled Synthetic C3a Protein as a Novel Fluorescent Probe for Human Complement C3a Receptor. *Bioconjugate Chem.* **2017**, *28* (6), 1669–1676. <https://doi.org/10.1021/acs.bioconjchem.7b00132>.
- (29) Rajendran, M.; Yapici, E.; Miller, L. W. Lanthanide-Based Imaging of Protein-Protein Interactions in Live Cells. *Inorg. Chem.* **2014**, *53* (4), 1839–1853. <https://doi.org/10.1021/ic4018739>.
- (30) Mohandessi, S.; Rajendran, M.; Magda, D.; Miller, L. W. Cell-Penetrating Peptides as Delivery Vehicles for a Protein-Targeted Terbium Complex. *Chem.-Eur. J.* **2012**, *18* (35), 10825–10829. <https://doi.org/10.1002/chem.201201805>.
- (31) Zou, X.; Rajendran, M.; Magda, D.; Miller, L. W. Cytoplasmic Delivery and Selective, Multicomponent Labeling with Oligoarginine-Linked Protein Tags. *Bioconjugate Chem.* **2015**, *26* (3), 460–465. <https://doi.org/10.1021/bc500550z>.
- (32) Kielar, F.; Congreve, A.; Law, G.; New, E. J.; Parker, D.; Wong, K.-L.; Castroño, P.; de Mendoza, J. Two-Photon Microscopy Study of the Intracellular Compartmentalisation of Emissive Terbium Complexes and Their Oligo-Arginine and Oligo-Guanidinium Conjugates. *Chem. Commun.* **2008**, No. 21, 2435–2437. <https://doi.org/10.1039/B803864C>.
- (33) Starck, M.; Fradgley, J. D.; Di Vita, S.; Mosely, J. A.; Pal, R.; Parker, D. Targeted Luminescent Europium Peptide Conjugates: Comparative Analysis Using Maleimide and Para-Nitropyridyl Linkages for Organelle Staining. *Bioconjugate Chem.* **2020**, *31* (2), 229–240. <https://doi.org/10.1021/acs.bioconjchem.9b00735>.
- (34) Montgomery, C. P.; Parker, D.; Lamarque, L. Effective and Efficient Sensitisation of Terbium Luminescence at 355 Nm with Cell Permeable Pyrazoyl-1-Azaxanthone Macrocyclic Complexes. *Chem. Commun.* **2007**, No. 37, 3841–3843. <https://doi.org/10.1039/b709805g>.
- (35) Pal, R.; Parker, D. A Ratiometric Optical Imaging Probe for Intracellular pH Based on Modulation of Europium Emission. *Org. Biomol. Chem.* **2008**, *6* (6), 1020–1033. <https://doi.org/10.1039/b718993a>.
- (36) Montgomery, C. P.; Murray, B. S.; New, E. J.; Pal, R.; Parker, D. Cell-Penetrating Metal Complex Optical Probes: Targeted and Responsive Systems Based on Lanthanide Luminescence. *Acc. Chem. Res.* **2009**, *42* (7), 925–937. <https://doi.org/10.1021/ar800174z>.
- (37) New, E. J.; Congreve, A.; Parker, D. Definition of the Uptake Mechanism and Sub-Cellular Localisation Profile of Emissive Lanthanide Complexes as Cellular Optical Probes. *Chem. Sci.* **2010**, *1* (1), 111–118. <https://doi.org/10.1039/c0sc00105h>.
- (38) Smith, D. G.; Pal, R.; Parker, D. Measuring Equilibrium Bicarbonate Concentrations Directly in Cellular Mitochondria and in Human Serum Using Europium/Terbium Emission Intensity Ratios. *Chem.-Eur. J.* **2012**, *18* (37), 11604–11613. <https://doi.org/10.1002/chem.201201738>.
- (39) Butler, S. J.; McMahon, B. K.; Pal, R.; Parker, D.; Walton, J. W. Bright Mono-Aqua Europium Complexes Based on Triazacyclononane That Bind Anions Reversibly and Permeate Cells Efficiently. *Chem.-Eur. J.* **2013**, *19* (29), 9511–9517. <https://doi.org/10.1002/chem.201301273>.
- (40) McMahon, B. K.; Pal, R.; Parker, D. A Bright and Responsive Europium Probe for Determination of pH Change within the Endoplasmic Reticulum of Living Cells. *Chem. Commun.* **2013**, *49* (47), 5363–5365. <https://doi.org/10.1039/C3CC42308E>.
- (41) Butler, S. J.; Lamarque, L.; Pal, R.; Parker, D. EuroTracker Dyes: Highly Emissive Europium Complexes as Alternative Organelle Stains for Live Cell Imaging. *Chem. Sci.* **2014**, *5* (5), 1750–1756. <https://doi.org/10.1039/C3SC53056F>.
- (42) Starck, M.; Pal, R.; Parker, D. Structural Control of Cell Permeability with Highly Emissive Europium(III) Complexes Permits Different Microscopy Applications. *Chem.-Eur. J.* **2016**, *22* (2), 570–580. <https://doi.org/10.1002/chem.201504103>.
- (43) Frawley, A. T.; Linford, H. V.; Starck, M.; Pal, R.; Parker, D. Enantioselective Cellular Localisation of Europium(III) Coordination Complexes. *Chem. Sci.* **2018**, *9* (4), 1042–1049. <https://doi.org/10.1039/C7SC04422D>.
- (44) Starck, M.; Fradgley, J. D.; Pal, R.; Zwier, J. M.; Lamarque, L.; Parker, D. Synthesis and Evaluation of Europium Complexes That Switch on Luminescence in Lysosomes of Living Cells. *Chem.-Eur. J.* **2021**, *27* (2), 766–777. <https://doi.org/10.1002/chem.202003992>.
- (45) Picot, A.; D'Aleo, A.; Baldeck, P. L.; Grichine, A.; Duperray, A.; Andraud, C.; Maury, O. Long-Lived Two-Photon Excited Luminescence of Water-Soluble Europium Complex: Applications in Biological Imaging Using Two-Photon Scanning Microscopy. *J. Am. Chem. Soc.* **2008**, *130* (5), 1532–1533. <https://doi.org/10.1102/ja076837c>.
- (46) D'Aleo, A.; Bourdolle, A.; Brustlein, S.; Fauquier, T.; Grichine, A.; Duperray, A.; Baldeck, P. L.; Andraud, C.; Brasselet, S.; Maury, O. Ytterbium-Based Bioprobes for Near-Infrared Two-Photon Scanning Laser Microscopy Imaging. *Angew. Chem., Int. Ed.* **2012**, *51* (27), 6622–6625. <https://doi.org/10.1002/anie.201202212>.
- (47) Grichine, A.; Haefele, A.; Pascal, S.; Duperray, A.; Michel, R.; Andraud, C.; Maury, O. Millisecond Lifetime Imaging with a Europium Complex Using a Commercial Confocal Microscope under One or Two-Photon Excitation. *Chem. Sci.* **2014**, *5* (9), 3475–3485. <https://doi.org/10.1039/C4SC00473F>.
- (48) Placide, V.; Bui, A. T.; Grichine, A.; Duperray, A.; Pitrat, D.; Andraud, C.; Maury, O. Two-Photon Multiplexing Bio-Imaging Using a Combination of Eu- and Tb-Bioprobes. *Dalton Trans.* **2015**, *44* (11), 4918–4924. <https://doi.org/10.1039/C4DT03115F>.
- (49) Bui, A. T.; Grichine, A.; Brasselet, S.; Duperray, A.; Andraud, C.; Maury, O. Unexpected Efficiency of a Luminescent Samarium(III) Complex for Combined Visible and Near-Infrared Biphononic Microscopy. *Chem.-Eur. J.* **2015**, *21* (49), 17757–17761. <https://doi.org/10.1002/chem.201503711>.

- (50) Bui, A. T.; Beyler, M.; Liao, Y.-Y.; Grichine, A.; Duperray, A.; Mulatier, J.-C.; Guennic, B. L.; Andraud, C.; Maury, O.; Tripier, R. Cationic Two-Photon Lanthanide Bioprobes Able to Accumulate in Live Cells. *Inorg. Chem.* **2016**, *55* (14), 7020–7025. <https://doi.org/10.1021/acs.inorgchem.6b00891>.
- (51) Bui, A. T.; Beyler, M.; Grichine, A.; Duperray, A.; Mulatier, J.-C.; Guyot, Y.; Andraud, C.; Tripier, R.; Brasselet, S.; Maury, O. Near Infrared Two Photon Imaging Using a Bright Cationic Yb(III) Bioprobe Spontaneously Internalized into Live Cells. *Chem. Commun.* **2017**, *53* (44), 6005–6008. <https://doi.org/10.1039/C7CC02835K>.
- (52) Bui, A. T.; Grichine, A.; Duperray, A.; Lidon, P.; Riobé, F.; Andraud, C.; Maury, O. Terbium(III) Luminescent Complexes as Millisecond-Scale Viscosity Probes for Lifetime Imaging. *J. Am. Chem. Soc.* **2017**, *139* (23), 7693–7696. <https://doi.org/10.1021/jacs.7b02951>.
- (53) Bui, A. T.; Roux, A.; Grichine, A.; Duperray, A.; Andraud, C.; Maury, O. Twisted Charge-Transfer Antennae for Ultra-Bright Terbium(III) and Dysprosium(III) Bioprobes. *Chem.-Eur. J.* **2018**, *24* (14), 3408–3412. <https://doi.org/10.1002/chem.201705933>.
- (54) Hamon, N.; Roux, A.; Beyler, M.; Mulatier, J.-C.; Andraud, C.; Nguyen, C.; Maynadier, M.; Bettache, N.; Duperray, A.; Grichine, A.; Brasselet, S.; Gary-Boho, M.; Maury, O.; Tripier, R. Pyclyen-Based Ln(III) Complexes as Highly Luminescent Bioprobes for In Vitro and In Vivo One- and Two-Photon Bioimaging Applications. *J. Am. Chem. Soc.* **2020**, *142* (22), 10184–10197. <https://doi.org/10.1021/jacs.0c03496>.
- (55) Pei, D.; Buyanova, M. Overcoming Endosomal Entrapment in Drug Delivery. *Bioconjugate Chem.* **2019**, *30* (2), 273–283. <https://doi.org/10.1021/acs.bioconjchem.8b00778>.
- (56) Brock, D. J.; Kondow-McConaghy, H. M.; Hager, E. C.; Pellois, J.-P. Endosomal Escape and Cytosolic Penetration of Macromolecules Mediated by Synthetic Delivery Agents. *Bioconjugate Chem.* **2019**, *30* (2), 293–304. <https://doi.org/10.1021/acs.bioconjchem.8b00799>.
- (57) Nadal-Bufí, F.; Henriques, S. T. How to Overcome Endosomal Entrapment of Cell-Penetrating Peptides to Release the Therapeutic Potential of Peptides? *Pept. Sci.* **2020**, *112* (6), e24168. <https://doi.org/10.1002/pep2.24168>.
- (58) Tietz, O.; Cortezon-Tamarit, F.; Chalk, R.; Able, S.; Vallis, K. A. Tricyclic Cell-Penetrating Peptides for Efficient Delivery of Functional Antibodies into Cancer Cells. *Nat. Chem.* **2022**, *14* (3), 284–293. <https://doi.org/10.1038/s41557-021-00866-0>.
- (59) LaRochelle, J. R.; Cobb, G. B.; Steinauer, A.; Rhoades, E.; Schepartz, A. Fluorescence Correlation Spectroscopy Reveals Highly Efficient Cytosolic Delivery of Certain Penta-Arg Proteins and Stapled Peptides. *J. Am. Chem. Soc.* **2015**, *137* (7), 2536–2541. <https://doi.org/10.1021/ja510391n>.
- (60) Marks, J. R.; Placone, J.; Hristova, K.; Wimley, W. C. Spontaneous Membrane-Translocating Peptides by Orthogonal High-Throughput Screening. *J. Am. Chem. Soc.* **2011**, *133* (23), 8995–9004. <https://doi.org/10.1021/ja2017416>.
- (61) O'Malley, W. I.; Abdelkader, E. H.; Aulsebrook, M. L.; Rubbiani, R.; Loh, C.-T.; Grace, M. R.; Spiccia, L.; Gasser, G.; Otting, G.; Tuck, K. L.; Graham, B. Luminescent Alkyne-Bearing Terbium(III) Complexes and Their Application to Bioorthogonal Protein Labeling. *Inorg. Chem.* **2016**, *55* (4), 1674–1682. <https://doi.org/10.1021/acs.inorgchem.5b02605>.
- (62) Cieslikiewicz-Bouet, M.; Eliseeva, S. V.; Aucagne, V.; Delmas, A. F.; Gillaizeau, I.; Petoud, S. Near-Infrared Emitting Lanthanide(III) Complexes as Prototypes of Optical Imaging Agents with Peptide Targeting Ability: A Methodological Approach. *RSC Adv.* **2019**, *9* (3), 1747–1751. <https://doi.org/10.1039/C8RA09419E>.
- (63) Leygue, N.; Picard, C.; Faure, P.; Bourrier, E.; Lamarque, L.; Zwier, J. M.; Galaup, C. Design of Novel Tripyridinophane-Based Eu(III) Complexes as Efficient Luminescent Labels for Bioassay Applications. *Org. Biomol. Chem.* **2022**, *20* (1), 182–195. <https://doi.org/10.1039/D1OB02092G>.
- (64) Overoye-Chan, K.; Koerner, S.; Looby, R. J.; Kolodziej, A. F.; Zech, S. G.; Deng, Q.; Chasse, J. M.; McMurry, T. J.; Caravan, P. EP-2104R: A Fibrin-Specific Gadolinium-Based MRI Contrast Agent for Detection of Thrombus. *J. Am. Chem. Soc.* **2008**, *130* (18), 6025–6039. <https://doi.org/10.1021/ja800834y>.
- (65) Heppeler, A.; Froidevaux, S.; Macke, H. R.; Jermann, E.; Behe, M.; Powell, P.; Hennig, M. Radiometal-Labelled Macrocyclic Chelator-Derivatised Somatostatin Analogue with Superb Tumour-Targeting Properties and Potential for Receptor-Mediated Internal Radiotherapy. *Chem.-Eur. J.* **1999**, *5* (7), 1974–1981. [https://doi.org/10.1002/\(SICI\)1521-3765\(19990702\)5:7<1974::AID-CHEM1974>3.0.CO;2-X](https://doi.org/10.1002/(SICI)1521-3765(19990702)5:7<1974::AID-CHEM1974>3.0.CO;2-X).
- (66) Eisenwiener, K.-P.; Powell, P.; Mäcke, H. R. A Convenient Synthesis of Novel Bifunctional Prochelators for Coupling to Bioactive Peptides for Radiometal Labelling. *Bioorg. Med. Chem. Lett.* **2000**, *10* (18), 2133–2135. [https://doi.org/10.1016/S0960-894X\(00\)00413-3](https://doi.org/10.1016/S0960-894X(00)00413-3).
- (67) Leclercq, F.; Cohen-Ohana, M.; Mignet, N.; Sbarbati, A.; Herscovici, J.; Scherman, D.; Byk, G. Design, Synthesis, and Evaluation of Gadolinium Cationic Lipids as Tools for Biodistribution Studies of Gene Delivery Complexes. *Bioconjugate Chem.* **2003**, *14* (1), 112–119. <https://doi.org/10.1021/bc025567e>.
- (68) Fremy, G.; Raibaut, L.; Cepeda, C.; Sanson, M.; Boujut, M.; Sénèque, O. A Novel DOTA-like Building Block with a Picolinate Arm for the Synthesis of Lanthanide Complex-Peptide Conjugates with Improved Luminescence Properties. *J. Inorg. Biochem.* **2020**, *213*, 111257. <https://doi.org/10.1016/j.jinorgbio.2020.111257>.
- (69) Placide, V.; Pitrat, D.; Grichine, A.; Duperray, A.; Andraud, C.; Maury, O. Design and Synthesis of Europium Luminescent Bio-Probes Featuring Sulfobetaine Moieties. *Tetrahedron Lett.* **2014**, *55* (7), 1357–1361. <https://doi.org/10.1016/j.tetlet.2014.01.025>.
- (70) Jagadish, B.; Ozumerzifon, T. J.; Roberts, S. A.; Hall, G. B.; Mash, E. A.; Raghunand, N. Improved Synthesis of 10-(2-Alkylamino-2-Oxoethyl)-1,4,7,10-Tetraazacyclododecane-1,4,7-Triace Tic Acid Derivatives Bearing Acid-Sensitive Linkers. *Synth. Commun.* **2014**, *44* (3), 441–449. <https://doi.org/10.1080/00397911.2013.813547>.
- (71) Horrocks, W. D.; Sudnick, D. R. Lanthanide Ion Luminescence Probes of the Structure of Biological Macromolecules. *Acc. Chem. Res.* **1981**, *14* (12), 384–392. <https://doi.org/10.1021/ar00072a004>.
- (72) Beeby, A.; Clarkson, I. M.; Dickins, R. S.; Faulkner, S.; Parker, D.; Royle, L.; Sousa, A. S. de; Williams, J. A. G.; Woods, M. Non-Radiative Deactivation of the Excited States of Europium, Terbium and Ytterbium Complexes by

- Proximate Energy-Matched OH, NH and CH Oscillators: An Improved Luminescence Method for Establishing Solution Hydration States. *J. Chem. Soc., Perkin Trans. 2* **1999**, No. 3, 493–504. <https://doi.org/10.1039/A808692C>.
- (73) Supkowski, R. M.; Horrocks, W. D. On the Determination of the Number of Water Molecules, *q*, Coordinated to Europium(III) Ions in Solution from Luminescence Decay Lifetimes. *Inorg. Chim. Acta* **2002**, *340*, 44–48. [https://doi.org/10.1016/S0020-1693\(02\)01022-8](https://doi.org/10.1016/S0020-1693(02)01022-8).
- (74) Walton, J. W.; Bourdolle, A.; Butler, S. J.; Soulie, M.; Delbianco, M.; McMahon, B. K.; Pal, R.; Puschmann, H.; Zwieter, J. M.; Lamarque, L.; Maury, O.; Andraud, C.; Parker, D. Very Bright Europium Complexes That Stain Cellular Mitochondria. *Chem. Commun.* **2013**, *49* (16), 1600–1602. <https://doi.org/10.1039/c2cc35247h>.
- (75) Dai, L.; Lo, W.-S.; Zhang, J.; Law, G.-L. One-Step Reaction for Screening of Chromophores to Improve the Luminescence of Lanthanide Complexes. *Asian J. Org. Chem.* **2017**, *6* (12), 1845–1850. <https://doi.org/10.1002/ajoc.201700403>.
- (76) Appelbaum, J. S.; LaRochelle, J. R.; Smith, B. A.; Balkin, D. M.; Holub, J. M.; Schepartz, A. Arginine Topology Controls Escape of Minimally Cationic Proteins from Early Endosomes to the Cytoplasm. *Chem. Biol.* **2012**, *19* (7), 819–830. <https://doi.org/10.1016/j.chembiol.2012.05.022>.
- (77) Macchi, S.; Signore, G.; Boccardi, C.; Di Rienzo, C.; Beltram, F.; Cardarelli, F. Spontaneous Membrane-Translocating Peptides: Influence of Peptide Self-Aggregation and Cargo Polarity. *Sci. Rep.* **2015**, *5*, 16914. <https://doi.org/10.1038/srep16914>.
- (78) Wissner, R. F.; Steinauer, A.; Knox, S. L.; Thompson, A. D.; Schepartz, A. Fluorescence Correlation Spectroscopy Reveals Efficient Cytosolic Delivery of Protein Cargo by Cell-Permeant Miniature Proteins. *ACS Cent. Sci.* **2018**, *4* (10), 1379–1393. <https://doi.org/10.1021/acscentsci.8b00446>.
- (79) Schwarzenbach, G.; Flaschka, H. *Complexometric Titrations*; Methuen: London, 1969.
- (80) Brouwer, A. M. Standards for Photoluminescence Quantum Yield Measurements in Solution (IUPAC Technical Report). *Pure Appl. Chem.* **2011**, *83* (12), 2213–2228. <https://doi.org/10.1351/PAC-REP-10-09-31>.
- (81) Resch-Genger, U.; Rurack, K. Determination of the Photoluminescence Quantum Yield of Dilute Dye Solutions (IUPAC Technical Report). *Pure Appl. Chem.* **2013**, *85* (10), 2005–2013. <https://doi.org/10.1351/PAC-REP-12-03-03>.
- (82) Sheldrick, G. M. SHELXT - Integrated Space-Group and Crystal-Structure Determination. *Acta Crystallogr. Sect. A* **2015**, *71*, 3–8. <https://doi.org/10.1107/S2053273314026370>.
- (83) Sheldrick, G. M. Crystal Structure Refinement with SHELXL. *Acta Crystallogr. Sect. C-Struct. Chem.* **2015**, *71*, 3–8. <https://doi.org/10.1107/S2053229614024218>.
- (84) Dolomanov, O. V.; Bourhis, L. J.; Gildea, R. J.; Howard, J. A. K.; Puschmann, H. OLEX2: A Complete Structure Solution, Refinement and Analysis Program. *J. Appl. Crystallogr.* **2009**, *42*, 339–341. <https://doi.org/10.1107/S0021889808042726>.
- (85) Knutsson, S.; Engdahl, C.; Kumari, R.; Forsgren, N.; Lindgren, C.; Kindahl, T.; Kitur, S.; Wachira, L.; Kamau, L.; Ekström, F.; Linusson, A. Noncovalent Inhibitors of Mosquito Acetylcholinesterase 1 with Resistance-Breaking Potency. *J. Med. Chem.* **2018**, *61* (23), 10545–10557. <https://doi.org/10.1021/acs.jmedchem.8b01060>.
- (86) Palasek, S. A.; Cox, Z. J.; Collins, J. M. Limiting Racemization and Aspartimide Formation in Microwave-Enhanced Fmoc Solid Phase Peptide Synthesis. *J. Peptide Sci.* **2007**, *13* (3), 143–148. <https://doi.org/10.1002/psc.804>.
- (87) Thieriet, N.; Alsina, J.; Giralt, E.; Guibe, F.; Albericio, F. Use of Alloc-Amino Acids in Solid-Phase Peptide Synthesis. Tandem Deprotection-Coupling Reactions Using Neutral Conditions. *Tetrahedron Lett.* **1997**, *38* (41), 7275–7278. [https://doi.org/10.1016/S0040-4039\(97\)01690-0](https://doi.org/10.1016/S0040-4039(97)01690-0).

Luminescent Peptide/Lanthanide(III) Complex Conjugates with Push-Pull Antennas: Application to One and Two-Photon Microscopy Imaging

Ji-Hyung Choi,^{a‡} Guillaume Fremy,^{ab‡} Thibault Charnay,^a Nour Fayad,^c Jacques Pécaut,^d Sule Erbek,^{ef} Niko Hildebrandt,^c Véronique Martel-Frchet,^{ef} Alexei Grichine^e and Olivier Sénèque^{*a}

^a Univ. Grenoble Alpes, CNRS, CEA, IRIG, LCBM (UMR 5249), F-38000 Grenoble, France.

^b Univ. Grenoble Alpes, CNRS, DCM (UMR 5250) F-38000 Grenoble, France.

^c Laboratoire COBRA (Chimie Organique, Bioorganique, Réactivité et Analyse), UMR 6014, CNRS, Université de Rouen Normandie, INSA, Mont-Saint-Aignan cedex 76821, France.

^d Univ. Grenoble Alpes, CEA, CNRS, IRIG, SyMMES, F-38000 Grenoble, France.

^e Univ. Grenoble Alpes, INSERM U1209, CNRS UMR 5309, Institute for Advanced Biosciences, F-38000 Grenoble, France.

^f EPHE, PSL Research University, 4-14 rue Ferrus, 75014 Paris, France

Email: olivier.seneque@cea.fr

‡ JHC and GF contributed equally to this work.

Supporting Information

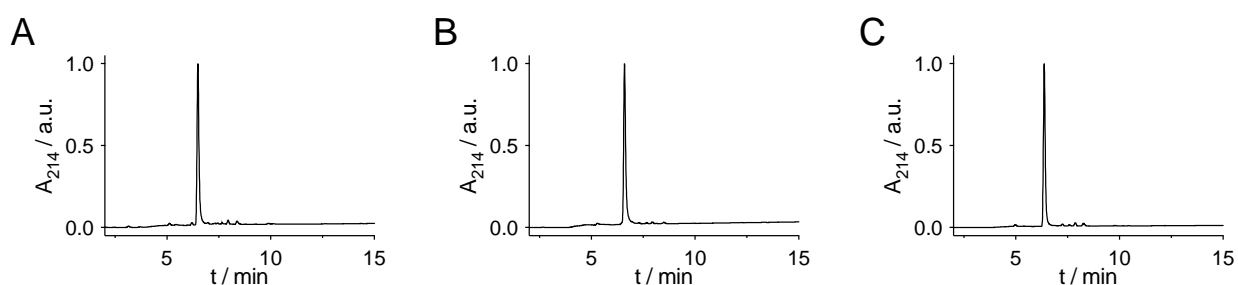


Figure S1. HPLC chromatograms (method B) of complexes (A) [Tb(L1)](Et₃NH), (B) [Eu(L1)](Et₃NH) and (C) [Dy(L1)](Et₃NH).

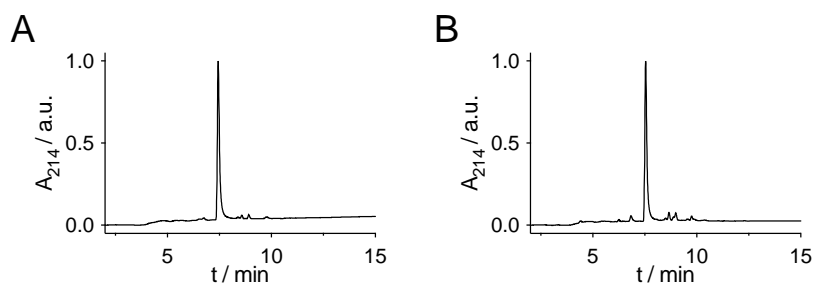


Figure S2. HPLC chromatograms (method B) of complexes (A) [Eu(L2)](Et₃NH) and (B) [Sm(L2)](Et₃NH).

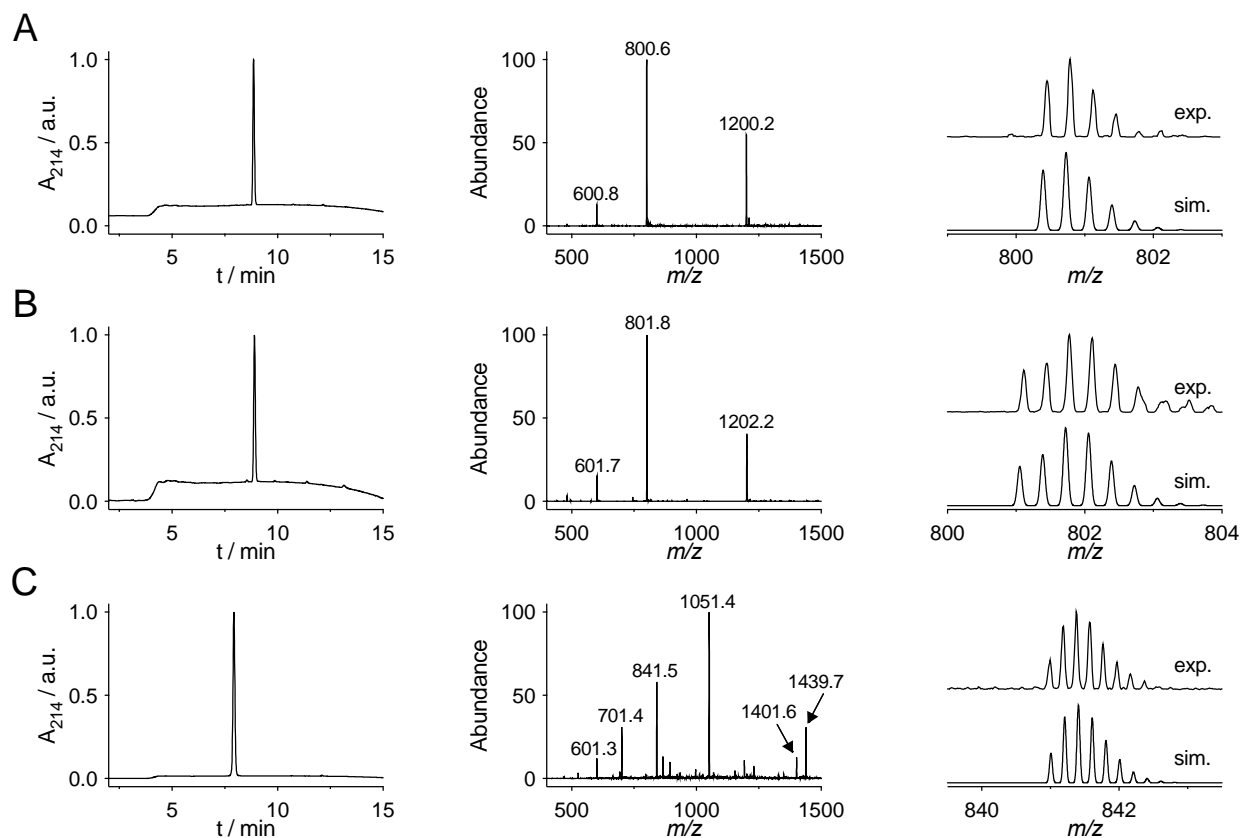


Figure S3. HPLC chromatograms (*left*) and LRMS (ESI⁺) spectra (*middle*: full MS spectrum; *right*: experimental and simulated isotopic pattern) obtained for (A) TP2[Tb(L1)], (B) TP2[Eu(L2)] and (C) ZF^{5.3}[Tb(L1)].

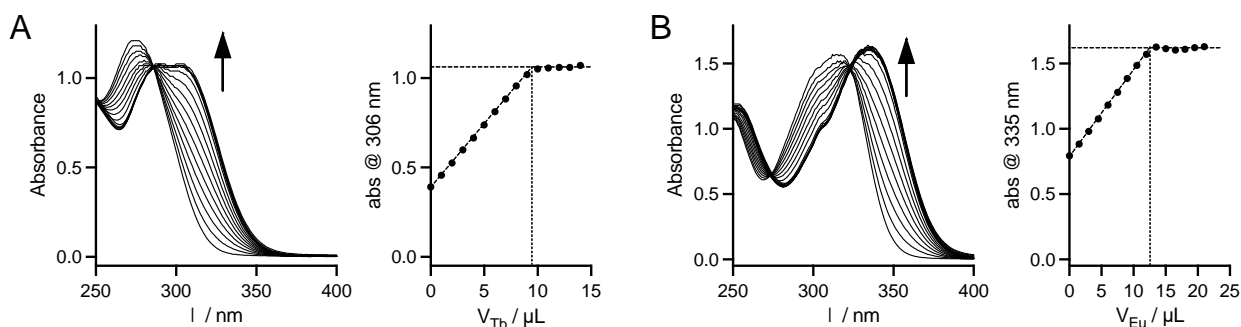


Figure S4. (A) Absorbance titration of L1 in HEPES buffer (10 mM, pH 7.5) by TbCl₃ in H₂O (23.1 mM). (B) Absorbance titration of L2 in HEPES buffer (10 mM, pH 7.4) by EuCl₃ in H₂O (11.0 mM). For both titrations, pathlength is 0.4 cm.

Table S1. Crystallographic data for **1**·NaBr and ([Tb(**L1**)]Na(H₂O)₃)₂.

Compound	1 ·NaBr	([Tb(L1)]Na(H ₂ O) ₃) ₂
Identification code	fg372	fg357
Empirical formula	C ₂₅ H ₃₈ BrIN ₅ NaO ₈	C ₃₀ H ₄₁ N ₅ NaO ₁₄ Tb
Formula weight	766.40	877.59
Temperature/K	150.05(10)	150.00(14)
Crystal system	monoclinic	triclinic
Space group	P2 ₁ /c	P-1
a/Å	12.35985(18)	11.5611(8)
b/Å	13.74070(16)	12.2940(11)
c/Å	18.3100(3)	15.9022(13)
α/°	90	103.926(7)
β/°	100.0683(15)	105.040(7)
γ/°	90	98.831(7)
Volume/Å ³	3061.75(8)	2061.6(3)
Z	4	2
ρ _{calc} /cm ³	1.663	1.414
μ/mm ⁻¹	2.419	1.789
F(000)	1544.0	888.0
Crystal size/mm ³	0.234 × 0.173 × 0.082	0.453 × 0.108 × 0.054
Radiation	Mo Kα (λ = 0.71073)	Mo Kα (λ = 0.71073)
2θ range for data collection/°	3.726 to 61.016	4.506 to 52.744
Index ranges	-17 ≤ h ≤ 17, -19 ≤ k ≤ 19, -26 ≤ l ≤ 26	-13 ≤ h ≤ 14, -12 ≤ k ≤ 15, -17 ≤ l ≤ 19
Reflections collected	71634	14403
Independent reflections	9350 [R _{int} = 0.0421, R _{sigma} = 0.0251]	8211 [R _{int} = 0.0782, R _{sigma} = 0.1221]
Data/restraints/parameters	9350/0/522	8211/0/476
Goodness-of-fit on F ²	1.061	0.987
Final R indexes [I ≥ 2σ (I)]	R ₁ = 0.0304, wR ₂ = 0.0642	R ₁ = 0.0665, wR ₂ = 0.1494
Final R indexes [all data]	R ₁ = 0.0401, wR ₂ = 0.0673	R ₁ = 0.0912, wR ₂ = 0.1642
Largest diff. peak/hole / e Å ⁻³	0.99/-0.62	2.92/-1.89